1 **Spatial-temporal distribution, photoreactivity and environmental**

2 **control of dissolved organic matter in the sea-surface microlayer of**

3 **the eastern marginal seas of China**

4 Lin Yang [a], Jing Zhang [a, c, *], Anja Engel [d], Gui-Peng Yang [a, b, c, *]

5 [a] Frontiers Science Center for Deep Ocean Multispheres and Earth System, and Key Laboratory of

6 Marine Chemistry Theory and Technology, Ministry of Education, Ocean University of China,

7 Qingdao 266100, China

8 [b] Laboratory for Marine Ecology and Environmental Science, Qingdao National Laboratory for

9 Marine Science and Technology, Qingdao 266237, China

10 [c] Institute of Marine Chemistry, Ocean University of China, Qingdao 266100, China

11 [d] GEOMAR Helmholtz Centre for Ocean Research, 24105 Kiel, Germany

[*] Corresponding authors. Key Laboratory of Marine Chemistry Theory and Technology, Ministry of Education, Ocean University of China, Qingdao 266100, China
E-mail addresses: zhangjouc@ouc.edu.cn (J. Zhang), gpyang@ouc.edu.cn (G.-P. Yang)
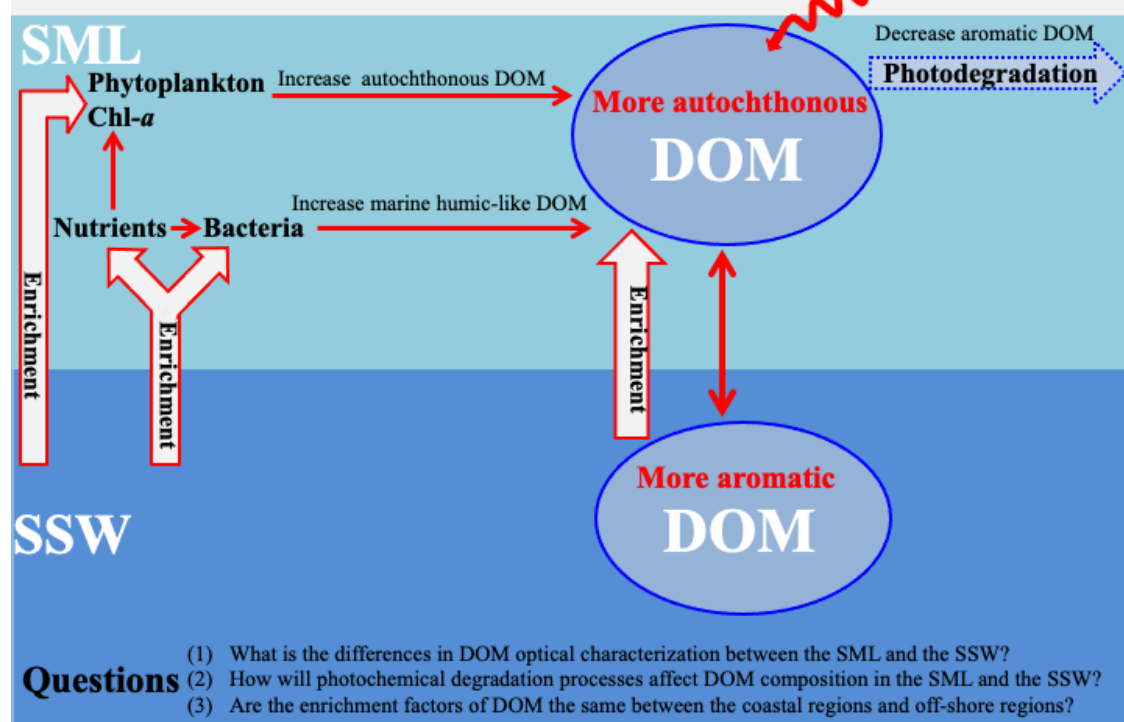
13   Graphical Abstract

14   **Abstract**

15   As the boundary interface between the atmosphere and ocean, the sea-surface microlayer (SML)

16   plays a significant role in the biogeochemical cycles of dissolved organic matter (DOM) and

17   macronutrients in marine environments. In our study, the optical properties of DOM were compared

18   between the SSW and the SML during spring, summer and winter in the East China Sea (ECS) and the

19   Yellow Sea (YS). In addition, photoexposure experiments were designed to compare photochemical

20   degradation processes of DOM between the SML and the SSW. Chromophoric DOM (CDOM),

21   fluorescent DOM, dissolved organic carbon, chlorophyll *a*, picoplankton, nutrients, and bacteria were

22   frequently enriched in the SML. The enrichment factors (EFs) of tryptophan-like component 4 was

23   significantly higher than other fluorescence components; the longer wavelength absorption values of

24   CDOM showed higher EFs in the SML, and the more significant relationship between CDOM and

25   Chl-a in the SML, indicating that autochthonous DOM was more strongly enriched in the SML than

26   the terrestrial DOM. Higher EFs were generally observed in the SML in the off-shore regions than in

27   the coastal regions, and CDOM in the SML was photobleached more after relatively strong irradiation,

28   as also indicated by the lower percentages of humic-like DOM and lower specific UV absorbance

29   values ($SUVA_{254}$) in the SML than the subsurface water (SSW). Compared to the SSW, the elevated

30   nutrients may stimulate phytoplankton growth, biological activity and then production of abundant

31   fresh autochthonous DOM in the SML. Our results revealed a new enrichment model for exploring the

32   air-sea interface environment, which can explain the more autochthonous properties of DOM in the

33   SML than the SSW.

35   **Keywords:** Sea-surface microlayer; Dissolved organic matter; Photochemical degradation;

36   Enrichment processes; Eastern marginal seas of China

1 Introduction

The sea-surface microlayer (SML) is the boundary interface between the atmosphere and the ocean, which covers about 70% of the Earth's surface. SML is physicochemically distinct from subsurface water (SSW, depth 3 ~ 5 m) and is characteristically enriched with phytoneuston, chlorophyll, particulate carbon, dissolved organic matter (Hardy 1982; Hardy and Apts, 1989), and biogenic organic compounds, such as lipids, proteins, and polysaccharides ((Liss and Duce, 1997; Liss and Duce, 2005). With a total thickness ranging between 1 μm and 1000 μm, the SML remains present in wind speeds of up to 13 m s^{-1} (Sabbaghzadeh et al., 2017). A variety of processes contribute to the formation of the SML in aquatic systems, these include but are not limited to, scavenging by rising bubbles, atmospheric deposition, dissolved organic matter (DOM) photochemical degradation and transformation, secretion, and biodegradation by organisms living within the microlayer (Neuston), and migration of motile organisms into the SML (Aller et al., 2005; Wotton and Preston, 2005). The SML is a very dynamic interface (Cunliffe et al., 2013), moreover, the impact of changes in UV radiation on air-sea fluxes in the SML of important trace gases need to be assessed. In addition, another uncertainty is whether photochemical reactions on the SML affect the flux of volatile species at the air-sea interface (Blough, 1997). Therefore, the role of the microlayer in oceanic emissions is not well understood and fundamental advance in understanding its properties are needed.

The processes leading to the enrichment of DOM in the SML are not solely controlled by changes in the DOM concentration at the sea surface microlayer, but are more complex (Mustaffa et al., 2018). Because of its unique position at the air-sea interface, the biological and photochemical reactions of DOM in the SML could strongly impact the biogeochemical cycling of biologically important

58 elements, for example, via the conversion of DOM into volatile species such as carbonyl sulfide

59 (OCS), which influence the atmospheric chemistry and climate (Mopper et al., 2002). Air-sea gas

60 exchanges of trace gases (e.g., CO, OCS, dimethylsulfide (DMS), and alkyl nitrates gases) can also be

61 greatly influenced by biological and photochemical reactions at the sea surface (Blough, 1997).

62   Optical measurements of absorbance and fluorescence have been applied to track DOM

63 variability in aquatic ecosystems (McKnight et al., 2001; Zepp et al., 2004; Coble, 2007). The fraction

64 of DOM that absorbs light in the ultraviolet and visible ranges of the electromagnetic spectrum and the

65 fraction that exhibits a blue fluorescence are known as chromophoric DOM (CDOM) and fluorescence

66 DOM (FDOM), respectively, and their relative compositions can provide information differentiating

67 between autochthonous and allochthonous sources (Coble, 1996; McKnight et al., 2001; Stedmon et

68 al., 2007). Photolysis of DOM promotes the formation of low-molecular-weight compounds,

69 increasing the bioavailability of biologically refractory materials and facilitating carbon uptake by

70 microbes (Kieber et al., 1989). Indices based on optical measurements of absorbance and fluorescence

71 are commonly used to track DOM composition and infer DOM processing due to their low analytical

72 cost and high throughput relative to molecular level analyses (Coble, 2007; Fellman et al., 2010;

73 Gabor et al., 2014). Recent studies have mainly focused on using the characteristics of CDOM as

74 indicators of the sources and degradation states of DOM (Massicotte et al., 2017) in the SSW, and its

75 vertical distribution in estuaries and open oceans (Yamashita et al., 2017; Margolin et al., 2018). In

76 addition, Mustaffa et al. (2018 and 2017) observed that FDOM enrichment in the SML in the coastal

77 regions and open Atlantic Ocean, and FDOM is frequently enriched during upwelling events in the

78 Baltic Sea.

79   Even though there are many studies that have documented the enrichment in DOM (e.g. amino

80   acids; carbohydrates) and inorganic nutrients in the SML relative to the SSW (Orellana et al., 2011;

81   Chen et al., 2016), the differences in organic matter composition between the SML and SSW, the

82   different enrichment factors of DOM in the SML between the coastal regions and the off-shore regions,

83   and how do photochemical degradation activities regulate DOM concentration in the SML need more

84   thorough discussion. Here, we investigated the concentration and composition of DOM in the SML

85   relative to the SSW and the responses of DOM to photoexposure. We hypothesized that the

86   photochemical reactions and enrichment processes could influence the composition difference of

87   DOM between the SML and the SSW, and greater solar exposure in the SML than in the SSW would

88   enhance the mineralization of DOM. To test these hypotheses, our study was designed to answer the

89   questions: (1) What is the differences in optical characterization of DOM between the SML and the

90   SSW? (2) Are the enrichment factors (EFs) of DOM the same between the coastal regions and

91   off-shore regions? (3) How will photochemical degradation processes affect DOM composition in the

92   SML and the SSW? We, therefore, compared the optical properties of DOM between the SSW and the

93   SML, and EFs of CDOM, FDOM components, dissolved organic carbon (DOC), chlorophyll-*a* (Chl-*a*),

94   nutrients, and bacterial abundance from the coastal waters to open ocean in the eastern marginal seas

95   of China (including the East China Sea (ECS) and the Yellow Sea (YS)) during spring of 2017 and

96   2019, summer of 2018, and winter of 2019; discuss how the composition of accumulated DOM was

97   affected by environmental conditions (wind speed and salinity) within the SML; and conducted

98   photoexposure experiments to compare photochemical degradation processes of DOM between the

99   SML and the SSW.

100

101   **2 Materials and methods**

 2.1 Study Area

     Four cruises were conducted during the four seasons, specifically, from: 27 March to 15 April

 2017 (R/V "*Dong Fang Hong 2*"), 26 June to 19 July 2018 (R/V "*Dong Fang Hong 2*"), March 2019

 (R/V "*Zheyu No. 2*"), and 28 December 2019 to 16 January 2020 (R/V "*Dong Fang Hong 3*"). The

 station locations are shown in Fig. 1. In spring, summer, and winter, SML samples were collected in

 the YS and the ECS, which are shallow seas located almost entirely on the continental shelf in the

 western Pacific Ocean where there is strong interaction between land and sea.
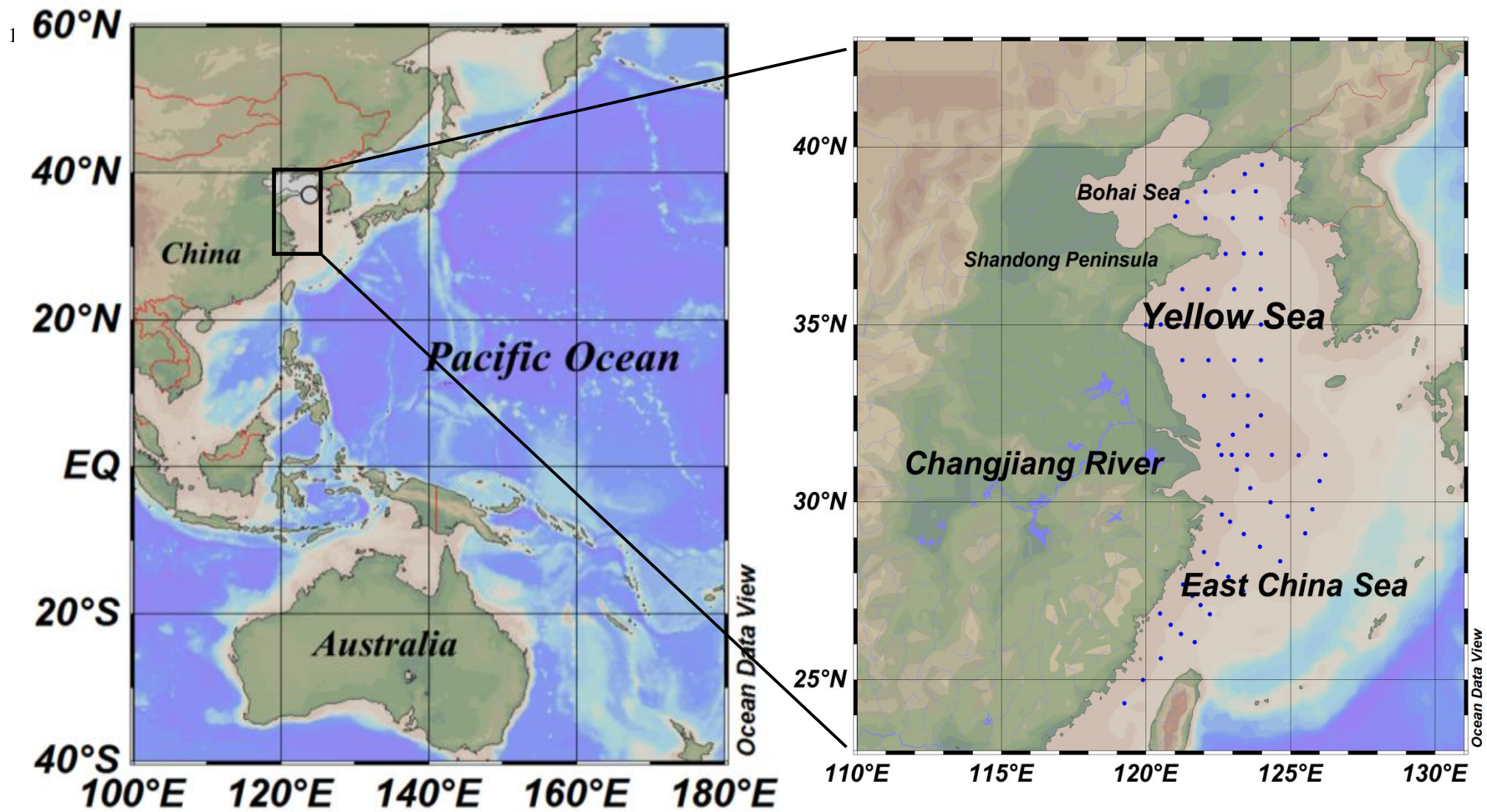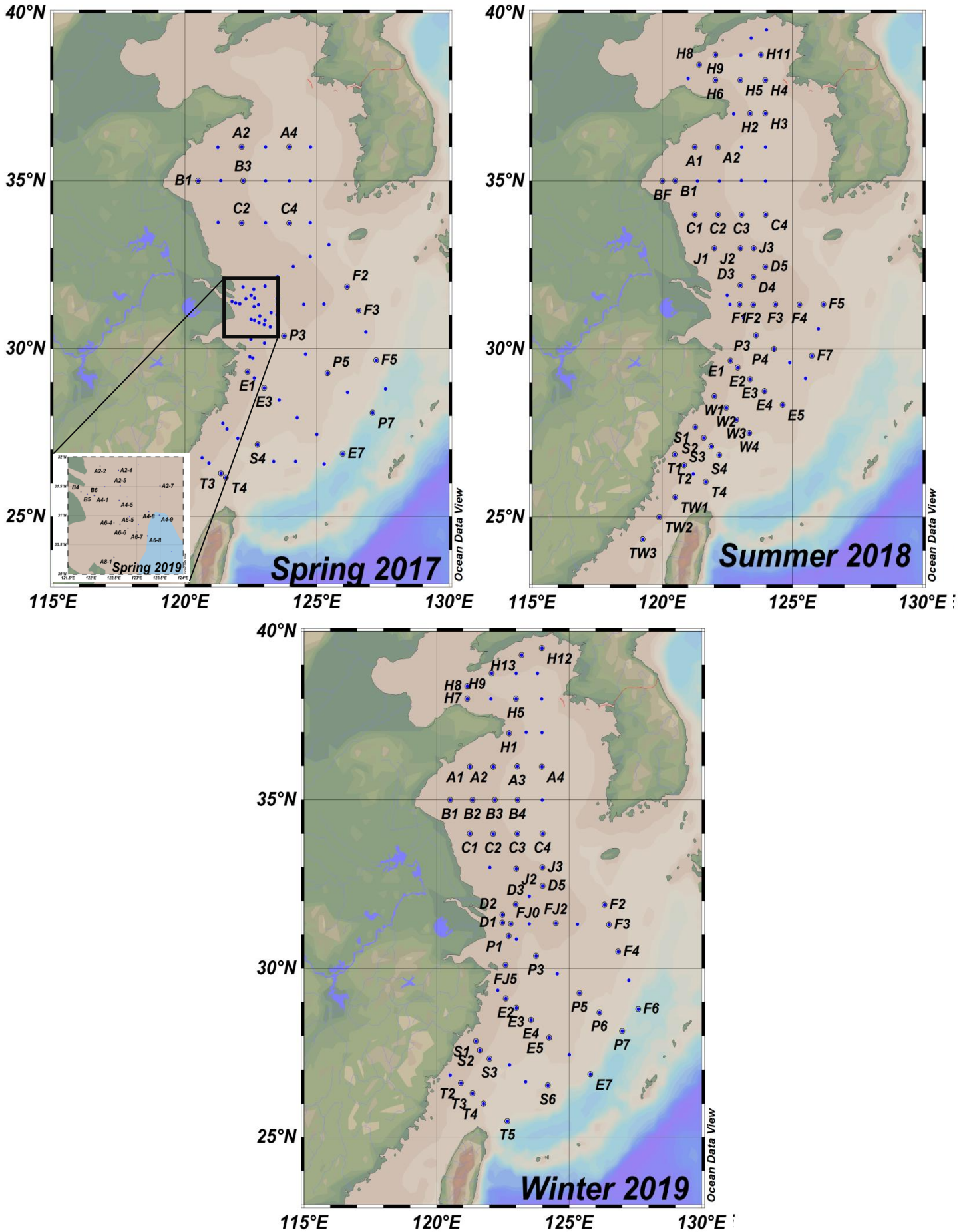
Fig. 1 Map of sampling stations.

112 *2.2 Sampling*

113   We collected 220 paired SML and SSW water samples. SSW samples were collected at 2–5 m

114 depth using 24 × 10-L Niskin bottles mounted on a rosette equipped with a

115 conductivity-temperature-depth (CTD) profiler. The SML samples were collected using the screen

116 sampling technique (Chen et al., 2016; Garrett, 1965) and were taken directly from the ship's bow

117 when conditions were calm. A screen sampler with a 1.6 mm mesh of stainless steel wire on a 40 cm ×

118 40 cm stainless steel frame was used. The SML samples were collected in 500 mL brown sample

119 bottles. The screen was held level and dipped into the sea surface, moved laterally in order to sample

120 from an undisturbed film, and then withdrawn slowly from the surface. Repeated dipping (11 times,

121 600 ml) was conducted until the desired volume was collected (the depth of the SML sample is nearly

122 300 ~ 1000 um). The screen method is often applied during field studies because of its relatively short

123 sampling time and large sample volume compared to other techniques (Momzikoff et al., 2004; Chen

124 et al., 2016). Immediately after collection, samples were filtered using 0.7 μm glass fiber filters (GF/F,

125 Whatmann) and the filtrates were transferred to 60 mL and 40 mL brown glass bottles (pre-cleaned

126 and pre-combusted) for later CDOM and DOC analyses. All samples were frozen (-20 ℃) and

127 protected from light, and upon arriving at the land laboratory, were analyzed as soon as possible. Sea

128 surface temperature and salinity were obtained from a Seabird 911 CTD Rosette. Meteorological data

129 (e.g., wind speed and air temperature) were recorded simultaneously by a ship-borne weather

130 instrument (Li et al., 2019).

131 *2.3 Photoexposure experiment*

132   SSW and SML water samples were collected in July 2018 at stations A3, BF, and H10 as well as

133 D2 and F6 located in the YS and the ECS, respectively. Samples (SSW: 2L; SML: 500 mL) were

134   immediately passed through 0.22 μm PES filters (Pall Corp. Port Washington, NY, USA) to remove

135   the majority of bacteria, placed in acid-washed and pre-combusted brown glass bottles and stored at

136   4 ℃. Similarly, filtered samples from each site were placed in five 80 mL optically transparent quartz

137   tubes (acid-washed and pre-combusted) and sealed without headspace or air bubbles to measure the

138   effect of light exposure. The quartz tubes were positioned on their sides under the irradiation source to

139   maximize the exposure of the sample; the water depth in each tube was 5 cm (i.e. the diameter of the

140   tube). Both sets (SML and SSW) were irradiated for 6, 12, 24, 50, and 88 h (25 ℃) in a GLZ-C

141   Quantum Sensor (Top Cloud-Agri Instrument, Zhejiang, China) solar simulator. All samples for DOC

142   concentration measurements were acidified to approximately pH 2.0 with high purity HCl and

143   analyzed within 7 d, and absorbance spectra and fluorescence excitation emission matrices (EEMs)

144   were run on non-acidified samples within 3 d of sampling (4 ℃ and dark).

145   *2.4 Analytical measurements*

146   *Determination of the CDOM absorption coefficient*

147   Absorption spectra were determined using a UV-visible spectrophotometer (UV-2550 bi-channel;

148   Shimadzu, Tokyo, Japan) equipped with two 10 cm path-length quartz cuvettes. Sample absorbance

149   was automatically corrected for the absorbance of Milli-Q water. Absorbance scans ranged from 200 to

150   800 nm, with a spectral resolution of 1 nm. The absorption coefficient of CDOM was calculated

151   according to equation (1):

152
$$a(\gamma) = 2.303A(\gamma)/l \qquad\qquad (1)$$

153   where, $A(\lambda)$ is the absorbance at wavelength λ; and r is the path length of the quartz cuvette in meters.

154   The spectral slope of the CDOM absorption curve (S) was calculated according to a non-linear

155   regression over the 275–295 nm and 350–400 nm wavelength range, according to:

156
$$a(\lambda) = a(\lambda_0)\exp[S(\lambda_0-\lambda)]+K \qquad\qquad (2)$$

157   where, $\alpha(\lambda)$ is the absorption coefficient at wavelength λ; $\alpha(\lambda_0)$ is the absorption at the reference

158   wavelength λ_0 of 440 nm; S is the spectral slope; and K is a background parameter that accounts for

159   baseline shifts or attenuation due to factors other than CDOM. S was measured in the wavelength

160   ranges of 275–295 nm ($S_{275-295}$, nm^{-1}) and 350–400 nm ($S_{350-400}$, nm^{-1}). $S_{275-295}$ is used to characterize

161   DOM, with high values generally indicative of low-molecular-weight DOM that are linked to

162   photochemical modification (Helms et al., 2008; Ortega-Retuerta et al., 2009). The spectral slope ratio

163   (S_R) was defined as the ratio of the two spectral slopes, $S_{275-295}$ to $S_{350-400}$. S_R is also a sensitive

164   indicator of photochemically induced changes in the molecular weight within the CDOM pool, with

165   increases in S_R suggesting stronger photochemical degradation (Helms et al., 2008; Ortega-Retuerta et

166   al., 2009). We used the absorption coefficient at 254 nm (a(254)) to determine the concentration and

167   distribution of CDOM in the SML from the eastern marginal seas of China. The specific UV

168   absorbance ($SUVA_{254}$) can be used to measure aromaticity (Weishaar et al., 2003) and molecular

169   weight (Chowdhury, 2013) of DOM, with higher values generally indicative of higher aromaticity.

170    $SUVA_{254}$ is calculated as dividing the absorbance at 254 nm by DOC.

171   *EEMs and determination of the CDOM fluorescence index*

172   EEMs were obtained using a F-4500 fluorescence spectrophotometer with a 1 cm quartz cuvette

173   (Shimadzu) (Hoge et al., 1993). The emission spectra were scanned every 5 nm from 250 nm to 550

174   nm, and at the excitation wavelengths between 200–400 nm at 5 nm intervals, with 5 nm slit widths

175   for the excitation and emission modes. The FL Toolbox, which was developed by Wade Sheldon

176   (University of Georgia) for MATLAB, was used to remove the Rayleigh and Raman scattering peaks

177   using the Delaunay triangulation method (Zepp et al., 2004). The fluorescence intensities of the

178   samples were corrected with Milli-Q water blank EEMs and then normalized to the water Raman

179   integrated area maximum fluorescence intensities (Ex/Em = 350 nm/365–430 nm, 5 nm bandpass)

180   (Coble et al., 1998; Singh et al., 2010). Raman units (RU) (Stedmon et al., 2007; Singh et al., 2010)

181   were used as the units for the Raman peak areas of water when the excitation wavelength of 350 nm

182   was used for correction. EEMs were modeled using PARAFAC in MATLAB 7.5 with the DOMFluor

183   toolbox (Stedmon and Bro, 2008).

$$X_{ijk} = \sum_{n=1}^{F} a_{in}\, b_{jn} c_{kn} + \varepsilon_{ijk}$$

184   (3)

185   where X_{ijk} is the fluorescence intensity of the ith sample at the kth excitation and jth emission

186   wavelengths; a_{in} is directly proportional to the concentration (scores) of the nth fluorophore in the ith

187   sample; b_{jh} and c_{kn} are the estimates of the emission and excitation spectra (loadings) of the nth

188   fluorophore at wavelengths j and k, respectively; F is the number of components (fluorophores); and

189   ε_{ijk} represents the unexplained variability of the model (Singh et al., 2010). Split-half analysis

190   validation was used to determine the number of fluorescent components. The fluorescence intensity of

191   each fluorescent component was evaluated (Fig. S2, Supporting Information, Table 1).

192   *Determination of DOC, chlorophyll-a, heterotrophic bacterial abundance, dissolved oxygen, and*

193   *other parameters*

194   Concentrations of DOC were determined using the Shimadzu TOC-V$_{CPH}$ total organic carbon analyzer

195   with an injection volume of 80 μL. The accuracy of the test was ensured by measuring a deep seawater

196   reference (Hansell Laboratory, University of Miami) every 10 samples. Two forms of reference water

197   have been developed for DOC analysis. Deep-ocean water, collected at 2600 m in the Sargasso Sea

198   and containing biologically refractory DOC, as well as low carbon water for testing instrument blanks

199   are available to the U.S. and international communities of aquatic chemists (Hansell, 2013;

200   measurement and analytical errors < 19%). The Chl-*a* concentration was determined by a fluorescence

201   spectrophotometer (7200-000, Turner Designs, CA) after extraction in 90% acetone based on the

202   procedure of Parsons et al. (1984). DO was determined by iodination using the Winkler titration

203   method (Carpenter, 1964), the endpoint was determined using starch as a visual indicator. Salinity and

204   temperature data were collected in situ by a conductivity-temperature-depth sensor. All phytoplankton

205   samples were enumerated in triplicate according to Specification for Oceanographic Survey (State

206   Bureau of Technical Supervision Bureau, 1992). Nutrient species concentrations were determined

207   using an automatic analyzer (QuAAtro, Seal Analytical, Germany) (Grasshoff et al., 2007). All

208   phytoplankton samples were enumerated in triplicate according to Specification for Oceanographic

209   Survey (State Bureau of Technical Supervision Bureau, 1992). Heterotrophic bacterial abundance was

210   measured by flow cytometry (Beckman Coulter FC500-MPL) as described by Marie et al. (1997).

211

Enrichment factors

The enrichment factor (EF) in the SML is defined as follows

$$EF = C_M / C_S \qquad (4)$$

where C_M is the concentration of any substance in the SML; and C_S is its concentration in the SSW. If

the EF of a substance is greater than 1.0, that substance is considered enriched, if it is less than 1.0, it

is considered depleted (Chen et al., 2016).

2.5 Statistical analyses

The correlation coefficient (*R*) and probability (*P*) values were used to evaluate the

goodness-of-fit. The correlation matrix, analysis of variance, and principal components analysis were

conducted with SPSS version 18.0 (SPSS Inc., Chicago, IL, USA) to determine the possible

relationships between the DOM parameters and environmental factors. A *P*-value ≤ 0.05 was

considered significant. Regression analyses between the optical parameters of DOM and several

biogeochemical parameters in the SSW and the SML samples were performed in the Table S1 and the

Table S2, respectively.

3. Results and discussion

3.1 Distribution and chemical characterization of DOM in the SSW of the eastern marginal seas of

China

The surface distributions of salinity, temperature, CDOM, DOC, Chl-*a*, and several optical

parameters in the study area during spring, summer and winter are shown in Fig. S3 (SSW)-S4 (SML)

(Supporting Information). There was a strong south-to-north temperature gradient, with warmer waters

233   in the ECS and cooler waters in the YS. Lower salinities were observed in the Changjiang Estuary and

234   coastal waters. The lowest mean wind speed was observed in the summer of 2018 (Table 2). In spring

235   and summer, the bacterial abundances were lower in the YS (spring mean concentration: 2.26×10^8

236   cells/L; summer mean concentration: 3.79×10^8 cells/L) than in the ECS (spring mean: 2.98×10^8

237   cells/L; summer mean: 7.64×10^8 cells/L), indicating that the warmer southern ECS had stronger

238   biological activity in the SSW.

239   The a(254) value ranged from 1.08 to 19.28 m^{-1} in the SML and from 0.82 to 14.23 m^{-1} in the

240   SSW during these three seasons. a(254) values in the Changjiang Estuary (spring: station D1 (4.13

241   m^{-1}); summer: station D2 (3.98 m^{-1}); winter: station D1 (3.14 m^{-1})) and the northern YS (spring: station

242   A2 (4.26 m^{-1}); summer: station H11 (5.37 m^{-1}); winter: station H12 (5.95 m^{-1})) were generally higher

243   than other stations. CDOM absorption values and DOC concentrations were decreased from the

244   inshore to the offshore stations (Fig. S3 c)-d)). There were significantly negative linear correlations

245   between salinity and a(254) in all cruises in the SSW ($p < 0.01$, Fig. 3), especially in the ECS,

246   implying that freshwater run-off and seawater mixing played a more important role in determining

247   CDOM distributions in the SSW. The strongest negative linear relationship observed between salinity

248   and a(254) was observed in winter when the influence of terrestrial input in this study region was

249   maximal. In addition, $SUVA_{254}$ ranged from 0.51 to 8.39 L mg C^{-1} m^{-1} in the SML. In comparison with

250   the SML, the SSW exhibited lower variability in $SUVA_{254}$ values from 0.63 to 5.39 L mg C^{-1} m^{-1}, with

251   higher values at the northern YS stations and Changjiang Estuary coastal stations (Fig. S3k)).

252   According to the $SUVA_{254}$ trends observed by Massicotte et al. (2017), the DOM composition we

253   observed in the SSW of the Changjiang Estuary ecosystem were more similar to the DOM measured in

254   freshwater ecosystems than in the ocean. $SUVA_{254}$ underwent a sharp decrease from the Changjiang

255 Estuary ecosystem to the southeastern ECS, suggesting that aromatic and/or highly conjugated DOM

256 moieties were degraded along the aquatic continuum from the Changjiang Estuary to the open ocean.

257 Higher $S_{275-295}$ values were also observed in some off-shore stations (Fig. S4i)). These comparisons

258 showed that the DOM pools of the Changjiang Estuary contained molecules that were more

259 HMW-DOM and contained more aromatic compounds, CDOM in the SSW of the southeastern ECS,

260 which was derived predominantly from an autochthonous origin (phytoplankton production and

261 bacterial activity), clearly showed the presence of organic matter freshly released into sea (Yang et al.,

262 2020). The detail of mixing behavior, biological and photolytic degradation of dissolved organic

263 matter in the East China Sea and the Yellow Sea were discussed in our previous paper (Yang et al.,

264 2020).

265

266 *3.2 Fluorescence signature and factors controlling the composition of FDOM components in the SSW*

267 *and the SML*

268   FDOM properties can be used as the sensitive indicator of DOM processing and water mass. Four

269 fluorescent components were identified by PARAFAC analysis with the DOM Fluor toolbox in

270 MATLAB 7.5 (Stedmon and Bro, 2008), hereafter named C1, C2, C3, and C4 (Fig. S2). The

271 humic-like C1 and C3 were categorized as two traditional types of humic-like fluorescent components

272 (Coble 1996). Component 1 had primary fluorescence excitation and emission peaks at 345 nm and

273 455 nm, respectively, which was similar to terrestrial humic-like fluorophores in the visible region

274 (peak C) (Osburn et al., 2012). Relative to C1, the fluorescence of C3 was blue-shifted and had

275 fluorescence peaks at 385 nm emission and 315 nm excitation. The microbial humic-like component

276 had a relatively shorter emission peak wavelength compared to the terrestrial humic-like PARAFAC

277   components previously identified in the open ocean (Catala et al., 2015). C2 exhibited Ex/Em maxima

278   at 255 nm/310 (375) nm, which could be considered tyrosine-like fluorescence (Stedmon et al., 2003)

279   and attributed to autochthonous and/or microbial FDOM. C4 had an excitation range of 280 nm with

280   an emission peak at 335 nm, which corresponded to peak T of the amino-acid-like fluorescence of

281   tryptophan, likely derived from in situ primary autochthonous substances and other fresh biological

282   sources (Coble, 1996). The tryptophan-like C4 and the humic-like C1 and C3 in the SSW were all

283   negatively correlated with salinity ($P < 0.01$, Table S1), but increased with the increasing DO level.

284   These suggested that water mixing and microbial activity were important factors in determining

285   geographical distributions of FDOM in the SSW (Breitburg, et al., 2018; Yamashita et al., 2017;

286   Galgani and Engel, 2016). Moreover, the geographical distribution of humic-like C1 and protein-like

287   components were more similar to that of the Chl-a concentration in the SML (Fig. 4 a, b, d). Such

288   relationships suggested that the production of protein-like and humic-like FDOM with phytoplankton

289   production and decay in the SML.

290   FDOM enrichment in the SML of all stations ranged between 0.5 and 11 (n = 225) and FDOM

291   was more frequently enriched (C1: 89.6%; C2: 73.2%; C3: 91.8%; C4: 93.4% of all samples) than

292   CDOM. The fluorescence intensity of the components in the SML samples decreased in the following

293   order: tryptophan-like > tyrosine-like > terrestrial humic-like > marine humic-like; whereas those in

294   the SSW samples decreased in the order: tyrosine-like > tryptophan-like > marine humic-like >

295   terrestrial humic-like. The tryptophan-like component (C4) was mostly enriched in the SML samples

296   with a median EF = 2.2 and a range from 0.2 and 8.0. The EF of C4 was clearly higher than other

297   components in all seasons (Fig. 6b)), especially in summer, and the FDOM composition in the SML

298   revealed a relatively higher proportion of autochthonous tryptophan-like FDOM than the SSW. It has

299 also been broadly recognized that tryptophan-like C4 in the particulate fraction is related to recent

300 primary production (Brym et al., 2014; Yamashita, 2014) and that phytoplankton excrete

301 tryptophan-like fluorophores (Romare-Castillo et al., 2010). Together, as already emphasized

302 previously, the variation observed for FDOM can be more related to that of Chl-a in the SML, these

303 observations suggested that the DOM enriched in the SML was made up of a relatively higher

304 proportion of marine autochthonous DOM than the SSW.

305

306 *3.3 DOM and biogenic molecules accumulation in the SML*

307 Up to 88% of our CDOM samples were enriched in the SML, with the median EF for a(254) of

308 1.3, ranging between 0.4 and 6.7. Concentrations of CDOM, FDOM, nutrients, bacterial abundance,

309 and Chl-*a* in the SML were correlated with their respective SSW concentrations (Fig. 5),

310 demonstrating that transport from the SSW to the SML is an important pathway. Furthermore, the

311 relatively higher CDOM absorption enrichment value in the SML were found at longer wavelengths

312 (Fig. 6a)) EF of a(355) > EF of a(254)). Marine DOM usually has higher absorption slope than

313 terrestrial DOM, and the higher slope (no matter it is $S_{320\text{-}412}$ or $S_{275\text{-}295}$), marine production of DOM

314 had the largest influence on the CDOM absorption properties in the longer wavelength range (Danhiez

315 et al., 2017) ($S_{320\text{-}412}$: DOM marine origin VS. $S_{275\text{-}295}$: terrestrial DOM).

316 Galgani and Engel (2016) also observed that amino acid-like fluorophores were highly enriched

317 in the SML, not only due to their amphiphilic properties, but also due to their local production in the

318 SML. Therefore, the marine local production might significantly affect the composition of DOM in the

319 SML. Additionally, the nutrients showed significantly higher EFs (NO_3^-: 3.41 $\pm$ 6.08, n = 41; NO_2^-:

320 3.57 $\pm$ 5.54, n = 52; PO_4^{3-}: 2.13 $\pm$ 2.74, n = 68; and SiO_3^{2-}: 6.53 $\pm$ 13.67, n = 13) than biological and

321 DOM parameters in the SML. The strong correlation between the SML and SSW concentrations of

322 NO$_2^-$, NO$_3^-$, and SiO$_3^{2-}$ (Fig. 5) showed that the similar fundamental drivers are probably at work in

323 both compartments for these nutrients. For example, dissolved substances, particles, and

324 microorganisms were brought to the interface by simple diffusion, rising bubbles (Jarvis, 1967),

325 convection, and upwelling from sediments and subsurface water, and at the same time, the microlayer

326 is also a sink for fallout from the atmosphere (Duce et al., 1976). In addition, we also observed the

327 significant positive relationship between a(254) and Chl-*a* ($R = 0.662$, $P < 0.01$) in the SML during

328 spring, and the positive relationship between the EF of PO$_4^{3-}$ and the EF of Chl-*a* ($R = 0.319$, $P = 0.01$,

329 Table 3). These observations indicated that spatial variation of CDOM concentrations were related to

330 Chl-a in the SML. The enrichment of inorganic nutrients would be an important factor influencing the

331 production and composition of phytoplankton-produced DOM (Carlson and Hansell, 2003) in the

332 SML. Therefore, phytoplankton growth, primary productivity rate, biological activity and marine

333 autochthonous DOM production would all be enhanced by the enriched nutrients in the SML.

334

335

336

337

338

339

340

341
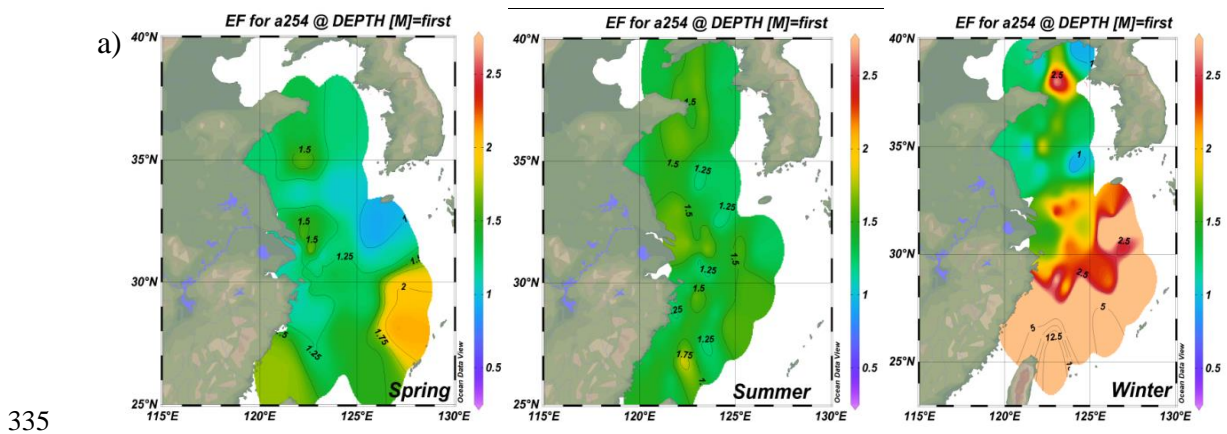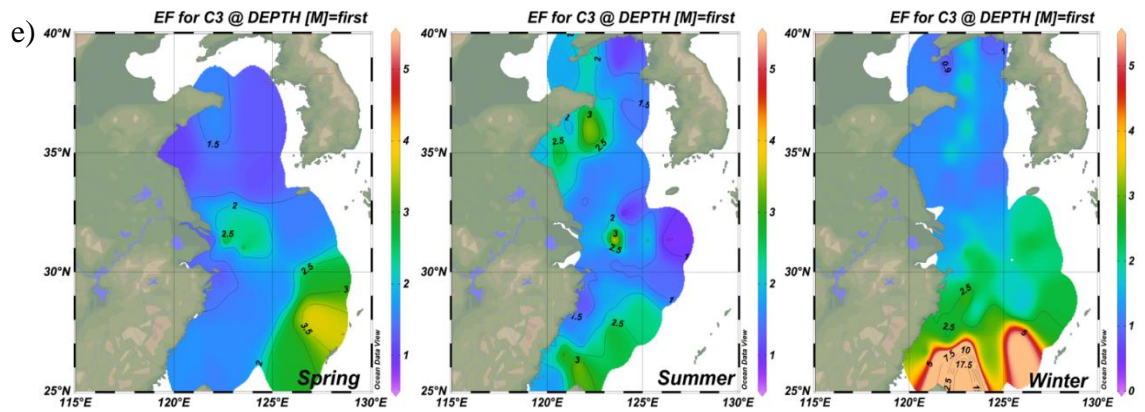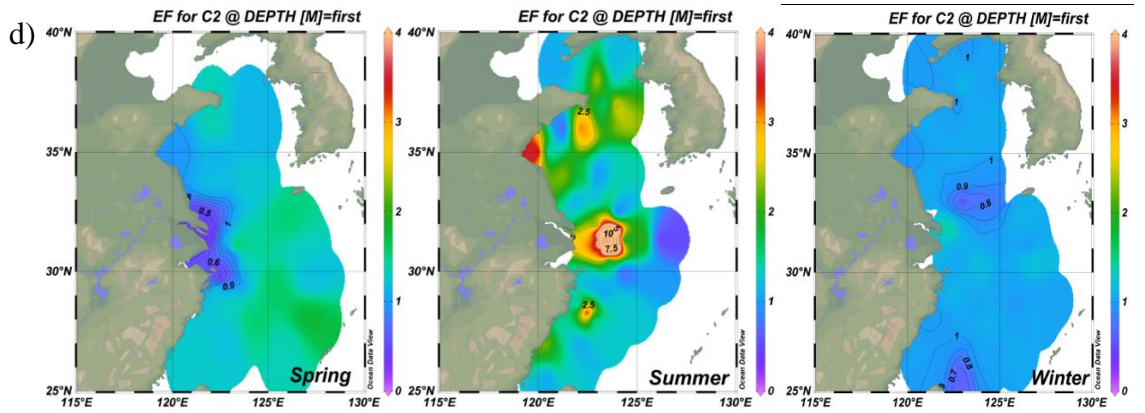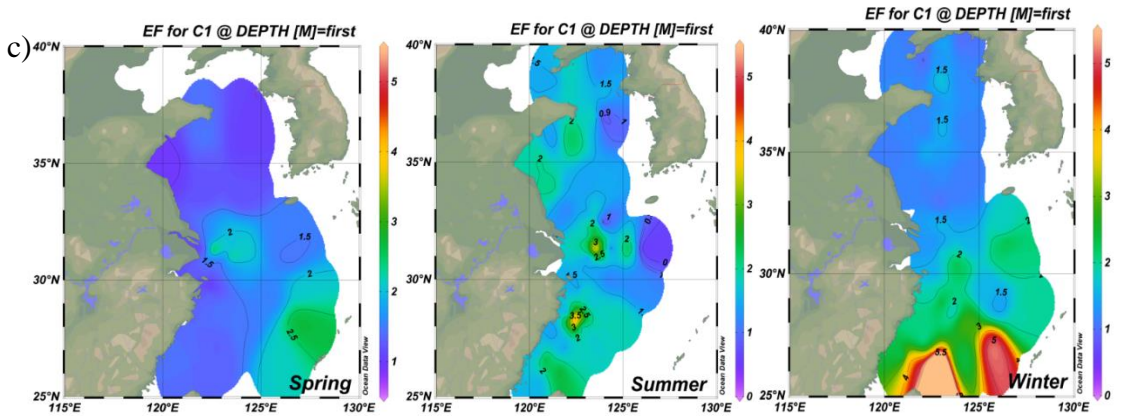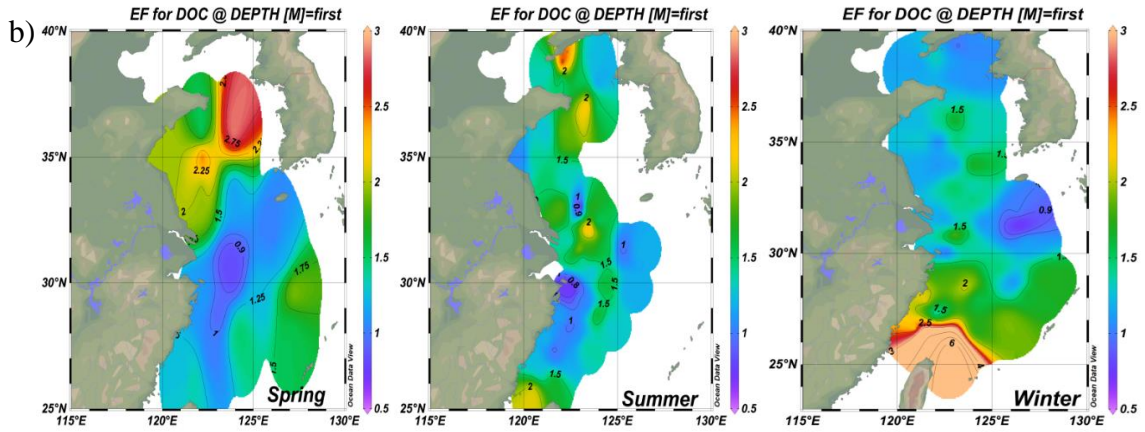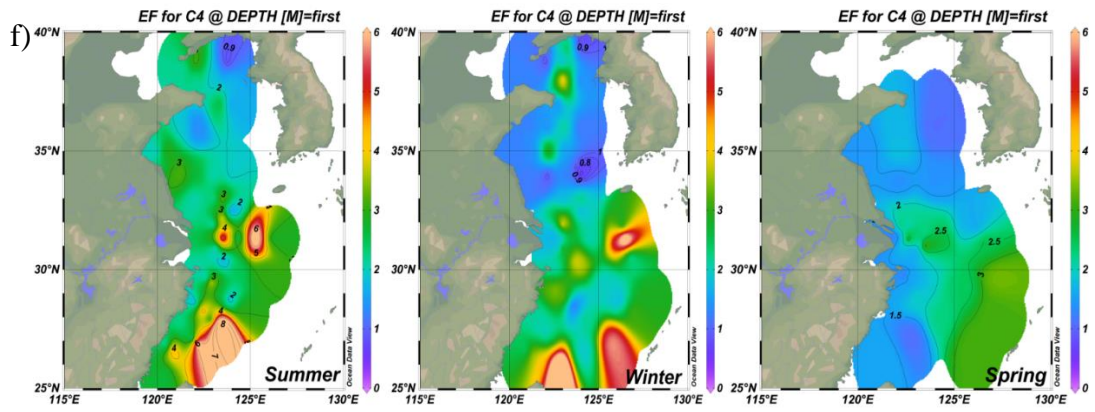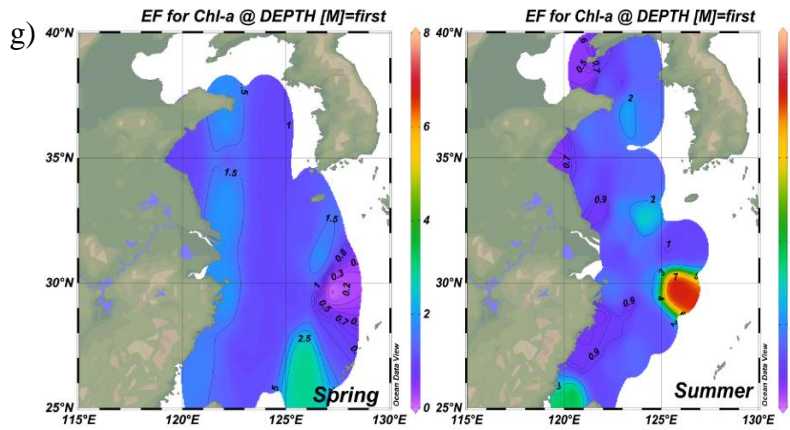
Fig. 2. Distributions of enrichment factors of CDOM, DOC, Chl-*a*, and four fluorescence components
in the surface microlayer water during spring, summer, and winter. Increasing DOM yields were
significant in coastal regions in all seasons, but the higher enrichment factors (EFs) were more
pronounced in off-shore regions.
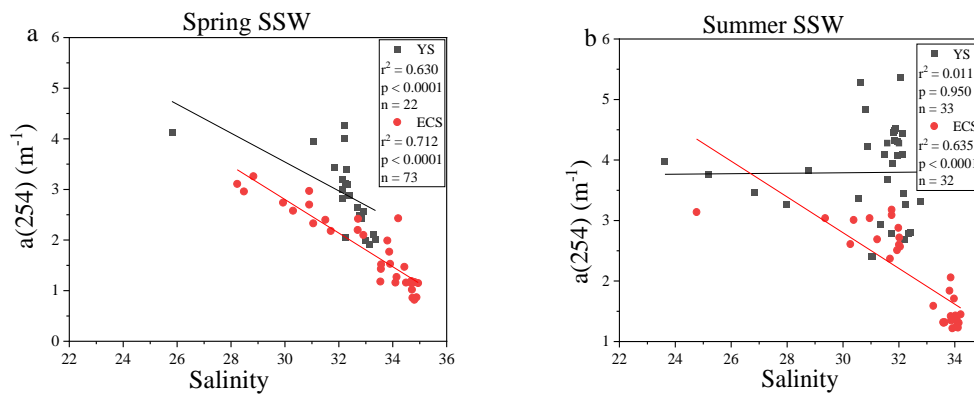
346
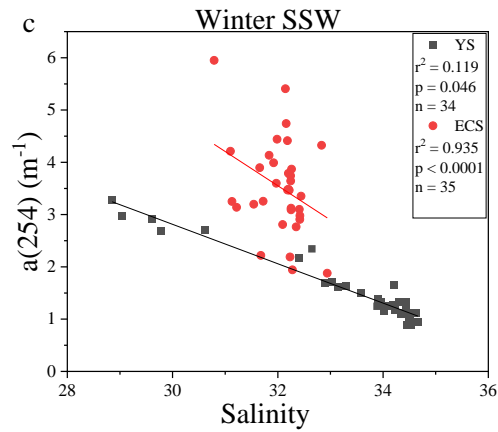
347

348 Fig. 3. Relationships between a(254) and salinity in the subsurface water (SSW) in the East China Sea

349 (ECS) and the Yellow Sea (YS) during spring, summer and winter.

350

351

352

353

354
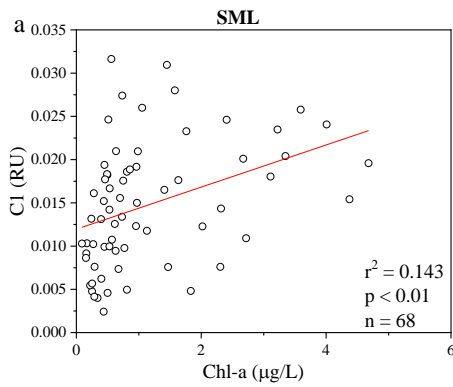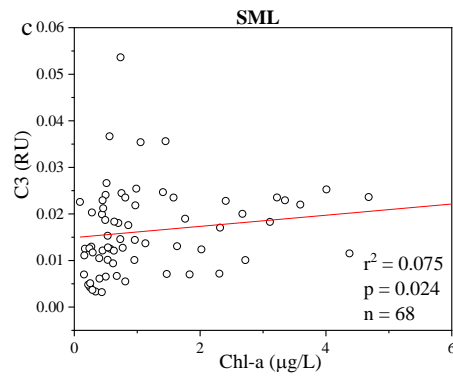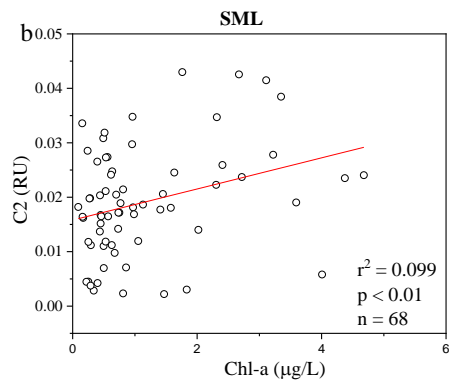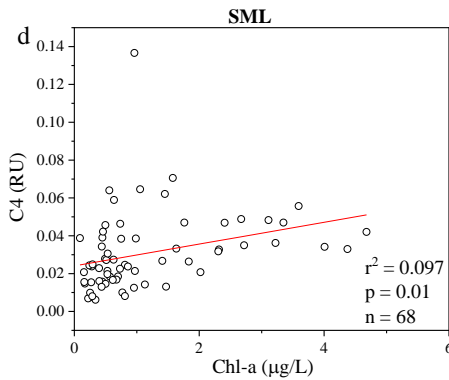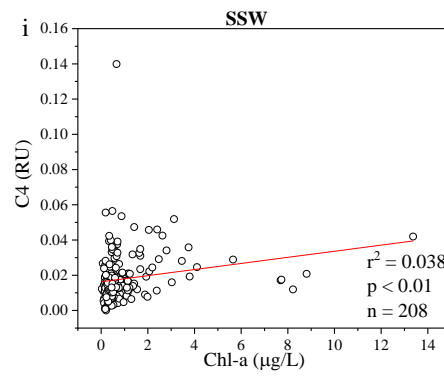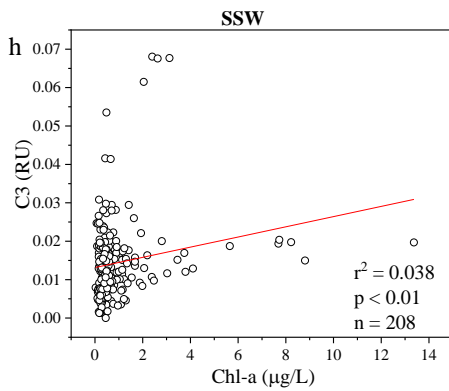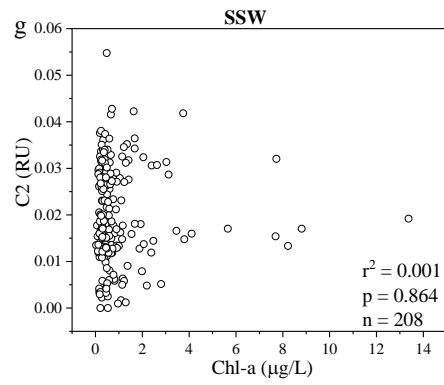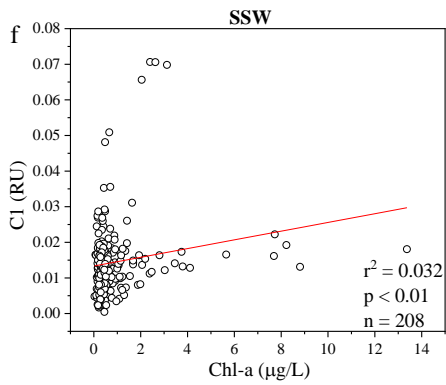
355 Fig. 4. Relationships between a(254), four fluorescence components and Chl-*a* in the sea-surface
356 microlayer (SML) (a-d) and in the SSW (f-i).

357

358

359

360

361

362
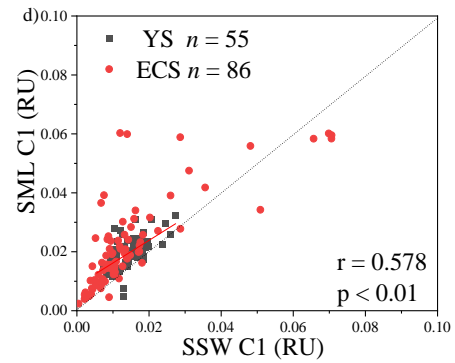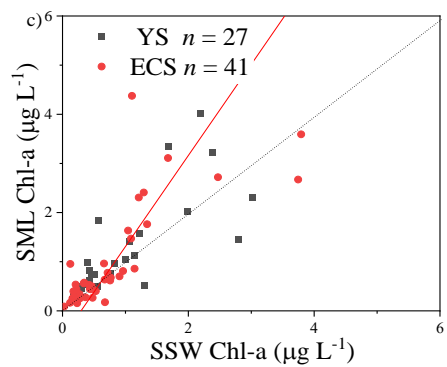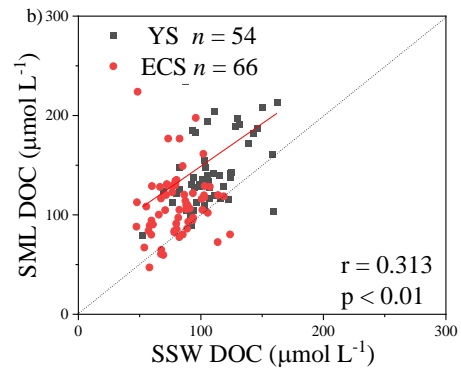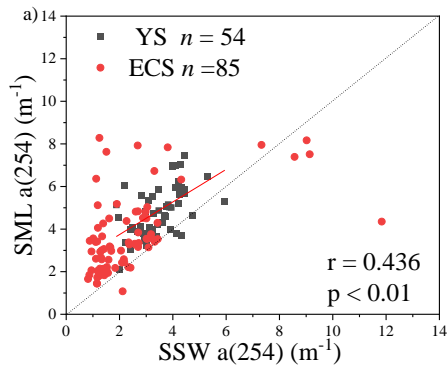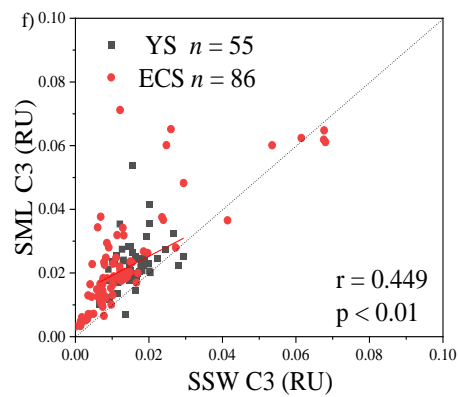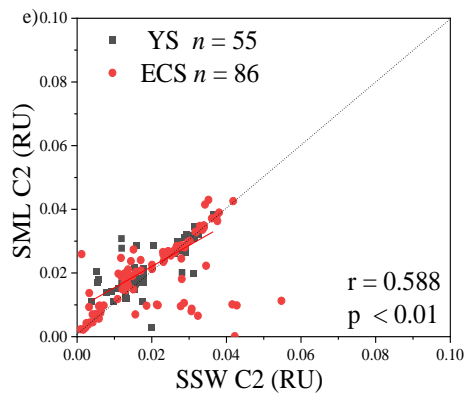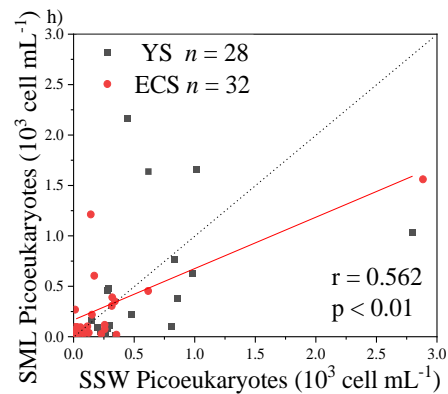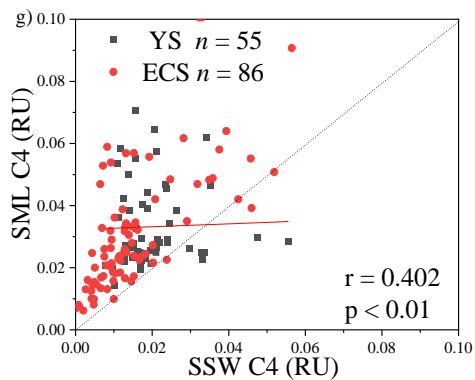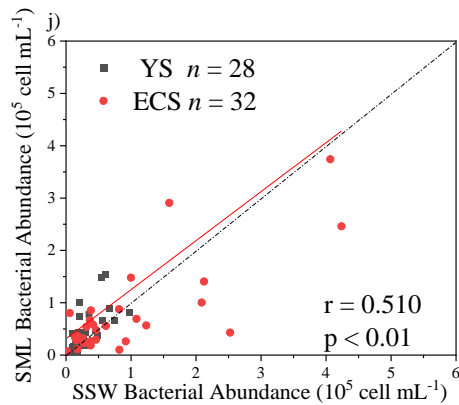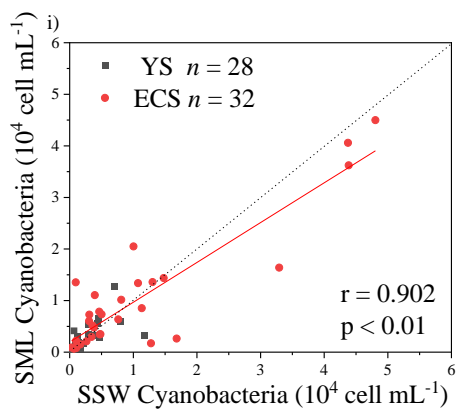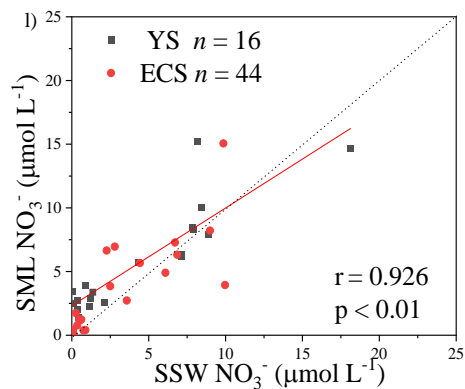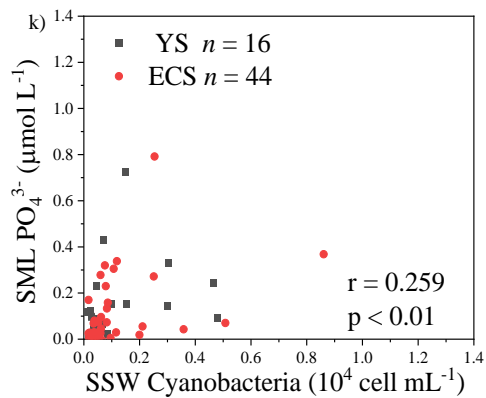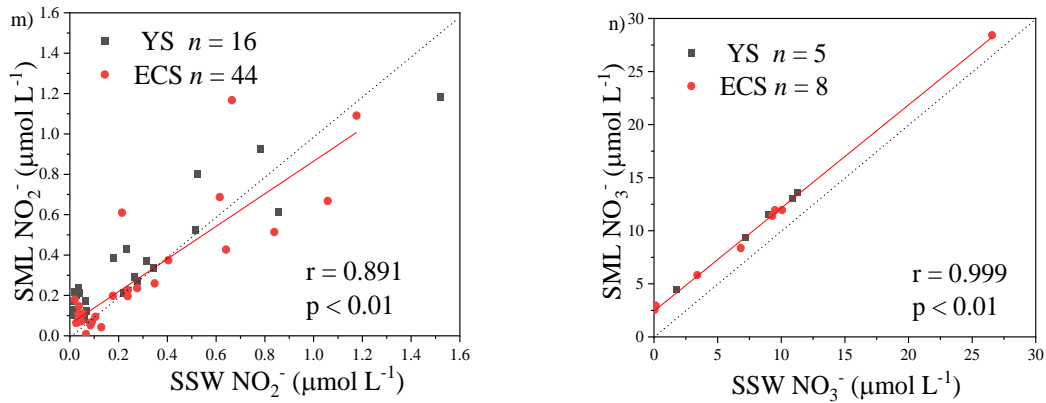
Fig. 5. Correlations between the microlayer CDOM, DOC, Chl-*a*, four fluorescence components concentrations, cyanobacteria, phytoplankton biomass, nutrients and bacterial abundance, and their subsurface water concentrations. The dashed lines correspond to the 1:1 lines, and the full lines are the regression models. (All DOM spectroscopic parameters sample were analyzed in spring, summer and winter; Chl-*a* was determined in spring, summer, and summer; cyanobacteria, phytoplankton biomass, nutrients and bacterial abundance were determined in spring and summer.).
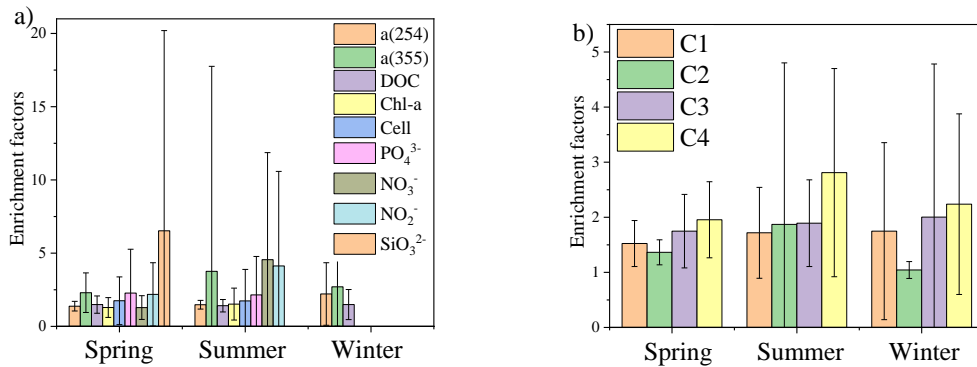
Fig. 6. Mean enrichment factor of a_{CDOM} (254 nm and 355 nm), DOC, Chl-*a*, nutrients (PO_4^{3-}; NO_3^-; NO_2^-, SiO_3^{2-}), and four fluorescence components during spring, summer, and winter.

3.4 Wind speed influencing the enrichment of DOM optical properties

The wind speeds during our observations ranged from 0.2 to 14.9 m s^{-1}. We divided them into three different wind regimes: low (0.0–2.0 m s^{-1}), moderate (2.0–10.0 m s^{-1}), and high (10.0–14.9 m s^{-1}). Although the EFs of DOC and Chl-*a* were negatively correlated with wind speed (DOC: $P = 0.002$; Chl-*a*: $P = 0.042$), the EFs of CDOM and FDOM were not. During the low wind regime, no significant relationships were apparent between wind speed and either EFs of CDOM or FDOM,

380   CDOM and FDOM were consistently enriched, with EFs ranging from 1.0 to 2.2, and a mean a(254)

381   EF value of 1.3 (n = 20). However, the EFs during moderate winds had larger variability and ranged

382   from 0.9 to 14.5, with a mean EF value of 1.6 (n = 143), and during high winds they ranged from 0.6

383   to 1.8, with a lower mean EF value of 1.1 (n = 18). In addition, depleted levels of CDOM (EF < 1)

384   occurred at frequencies of 5.6%, 9.1%, and 20.0% during low, moderate, and high wind regimes,

385   respectively. Therefore, although lower wind speeds and ascending bubbles might further promote the

386   transportation of organic materials from the underlying waters, DOM enrichments were still observed

387   at wind speeds up to > 10 m s^{-1}. Reinthaler et al. (2008) also reported that higher enrichment was

388   found at higher wind speeds. During moderate to high wind regimes, breaking waves not only can

389   disrupt the surface film and physically drive DOM back into the bulk water, but also facilitate the

390   formation of the SML as rising bubble plumes transported DOM to the surface, resulting in wider

391   ranges of EFs (Frew et al., 2004). Higher wind speed does enhance mixing (Reinthaler et al., 2008),

392   which can arguably favour transport of nutrients and DOM from the SSW equally (Wurl et al., 2011).

393   Although wind speed appear to play an important role in the enrichment of surface-active DOM, the

394   chemical composition of the SML influence its stability. For example, enrichments of sulphate

395   half-ester groups in the SML (Wurl and Holmes, 2008) could increase stability because these groups

396   can influence the intrinsic viscosity of marine polymers (Nichols et al., 2005) and sulphur-containing

397   algal carbohydrates are less soluble and hydrolysable (Kok et al., 2000). Sampling needs to be

398   performed on the leeward side of the boat with the boat moving into the wind to aboid contamination.

399   Although some disturbance of SML integrity was produced by the ship's movement and potential

400   contamination at high wind speeds and tidal mixing. It has long been known that the SML reforms

401   rapidly following physical disruption (Dragcevic and Pravdic, 1981). Rapid SML recovery occurs

402   because SML organics dispersed by breaking waves readily reabsorb to the surfaces of rising bubbles

403   generated by the same breaking waves (Woolf, 2005). Enrichment processes and biochemical

404   processes of organic substances in the marine environment are all likely to be the more important

405   contributors of DOM to the SML in our study regions.

406   *3.5 Photochemical degradation of DOM in the SSW and the SML*

407   Photobleaching is one of the major mechanisms determining the geographical distributions of

408   chromophoric and fluorescent DOM in the ocean (Helms et al., 2008; Brinkmann et al., 2003; Siegel

409   et al., 2005). The average $SUVA_{254}$ values in SSW were generally higher than those in the SML in our

410   study regions (SSW: 2.45 ± 0.91 L mg-C^{-1} m^{-1} vs. SML: 2.39 ± 1.34 L mg-C^{-1} m^{-1}), and the most

411   obvious distinction happened in summer (Table 2). These indicated that although CDOM

412   concentration in the SSW was lower than that in the SML, CDOM in the SSW has a higher degree of

413   aromaticity compared to the SML. Thus we performed photochemical incubation experiments to

414   confirm whether photochemical reactions influenced the differentiated aromaticity and photo-reactive

415   features of DOM between the SML and the SSW.

416   After 88 h of exposure, the a(254) values were only 49.6%, 45.5%, 42.1%, 41.8% and 37.0% of

417   the initial values at stations A3, BF, D2, F6, and H10 in the SSW, and 72.5%, 42.4%, 42.6%, 49.0%

418   and 44.0% of the initial values at stations A3, BF, D2, F6, and H10 in the SML, respectively. Overall,

419   a(254) and $SUVA_{254}$ decreased by $49.9 \pm 12.8\%$ and $43.0 \pm 15.5\%$, respectively, in the SML, and by

420    $56.8 \pm 4.7\%$ and $56.0 \pm 10.2\%$, respectively in the SSW. Therefore, stimulated solar UV exposure

421   caused a larger decrease in DOM absorbance in the SSW than the SML (Fig. 7). The relatively rapid

422   decrease of $SUVA_{254}$ in the SSW indicated a more rapid conversion of DOM to less humic-type

423   materials than in the SML. Although photodegradation causes CDOM absorption to decrease, DOC is

424   not sensitive to photodegradation in our photodegradation experiments (Fig. 7), implying that the light

425   exposure preferentially removed the colored DOM rather than the non-colored DOM (Bittar et al.,

426   2015). Approximately 65% of FDOM was lost during the irradiation experiment, except in the case of

427   the tyrosine-like component 2 from the SML at the station H10, which increased slightly.

428   Photoproduction of tyrosine-like components has been previously reported by Zhu et al. (2017), who

429   suggested that the photochemical degradation of CDOM contributed to the release small amounts of

430   tyrosine-like fluorophores. The tryptophan-like C4, humic-like C1 and C3 were more photodegradated

431   in the SSW than in the SML (Fig. 7c), e), f)). For example, C1, C3 and C4 show a marked decrease in

432   the SSW at the off-shore station F6. Because of the origin of CDOM at the station F6 remote from the

433   direct terrestrial influence, the majority of CDOM at the station F6 was thought to be a by-product of

434   net primary production. The present results showed that a large fraction of the total CDOM in the

435   SSW at the off-shore station F6 is still potentially sensitive to photooxidation. As already referred

436   previously, CDOM in the SSW showed higher $SUVA_{254}$ values, and higher percentages of humic-like

437   DOM than in the SML. Therefore, the photochemically mediated shifts in DOM in the SSW were

438   more pronounced than those in the SML in our incubation experiments, in terms of both absorption

439   and fluorescence values.

440   This heterogeneity in the EFs and photochemical reactivities of FDOM components can be

441   related to the chemical and structural nature, such as molecular weight, aromaticity or humification of

442   FDOM enrichment processes. Hydrophilic, carboxylic acid-bearing DOM moieties are preferentially

443   degraded by simulated sunlight (Brinkmann et al., 2003). The largest fractions of photolabile DOM are

444   made up of aromatic carbon rings or high double bond equivalent molecules (Kujawinski et al., 2004;

445   Gonsior et al., 2009). The humic-like C1 and C3, all of which exhibited significantly positive

446   relationships with SUVA$_{254}$ (< 0.001, Table 1) and shown higher aromaticity, were more prone to

447   photochemical degradation (Fig. 7c), e), and f)). The tyrosine-like C2, as compared to other

448   protein-like compounds, is generally considered more labile and susceptible to bacterial cycling and

449   rapid consumption by microbiota (Medeiros et al., 2015). The SML experiences the most intense solar

450   radiation, especially ultraviolet (UV) light (Obernosterer et al., 2005). Photochemical degradation may,

451   therefore, be a sink for aromaticity fluorescent components in the SML, and be a source for the

452   tyrosine-like C2. In addition, Blough (1997) discovered that photochemical production rates in the

453   SML should lead to the more rapid oxidative turnover of materials at the interface and potentially to

454   reactions and processes not observed in bulk waters. Therefore, differences in SUVA$_{254}$ values and

455   photoreaction behavior between the SSW and the SML may also reflect that DOM in the SML was

456   already photobleached, which resulted in the decrease of DOM aromaticity, CDOM in the SSW

457   appeared to be more susceptible to photochemical degradation than CDOM in the SML. Together,

458   photo-irradiation have the significant influence on the accumulation of protein-like DOM and

459   depletion of aromatic organic compounds in the SML, and organic carbon might have undergone a

460   more rapid cycling in the SML than the SSW.
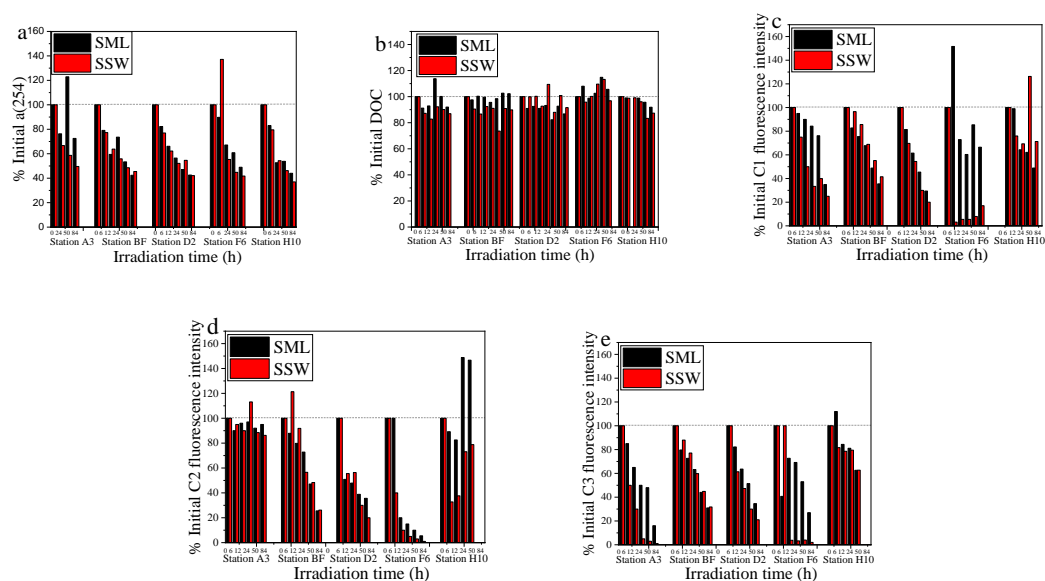
461

462
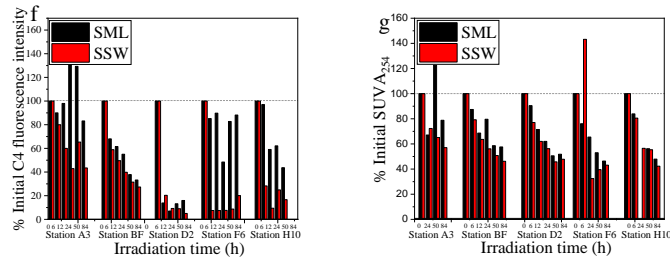
Fig. 7. Changes in ratios of a(254), DOC, SUVA$_{254}$ and four fluorescence components intensities to initial values for both SML and SSW sample.

3.6 Variations in the enrichment factors of CDOM, DOC, FDOM along the coastal regions to ocean

The concentrations of a(254) and DOC decreased from the coastal regions to the open ocean, and decreased from the northern part of the sampling area (the YS) to the southern part of the sampling area (the ECS) in both the SSW and the SML (Fig. S3 c)-d) and Fig. S4 a)-b)). However, CDOM and FDOM were more frequently enriched in the ECS (CDOM: 93% of all samples; FDOM: 72–94% of all samples) than that in the YS (CDOM: 86% of all samples; FDOM: 70–92% of all samples). The higher EF values for CDOM, FDOM, DOC, Chl-*a*, nutrients, and cell were generally observed in the ECS (Fig. 2). Lower EFs and EFs < 1, which indicate a depletion of CDOM in the SML, were usually observed at short distances from the coast (Fig. 2) with lower salinity. The salinity during our observations ranged from 23.6 to 35.1. Although CDOM and FDOM concentration negatively correlated with salinity, the EFs of CDOM and FDOM were weakly positive related with salinity (Fig. 8). The EFs of Chl-*a* and nutrient were also higher in the southeastern ECS (Fig. 2 and Fig. S5), where sufficient light and higher temperature combined to facilitate primary production and higher contributions of autochthonous materials to DOM. DOM in the SSW of the southern ECS was more dominated by marine autochthonous materials in our previous discussion (Yang et al., 2020). The Changjiang River discharges enormous amounts of N and P into the ECS (Liu et al., 2018), but

483 phosphorus is generally the major limiting element for phytoplankton growth in the ECS (Liu et al.,

484 2016). Thus the difference in EFs of CDOM and Chl-a between YS and the ECS, and between the

485 coast and off-shore regions is likely due to the significantly nutrients enrichment in the SML in the

486 off-shore regions. In winter, we observed especially higher EF values for CDOM and FDOM in the

487 southern ECS (Fig. 2a)-f)). With wind from the northwest (Weng et al., 2011), biologically essential

488 trace elements and anthropogenic emissions are carried from the land and can enter the ocean via the

489 SML by wet or dry deposition. The EFs of humic-like C1 and C3 were relatively high in winter (Fig.

490 6b)), probably due to the input from atmospheric deposition during winter, and the relatively low

491 CDOM concentrations in bulk water. Atmospheric deposition of organic carbon and nutrients were

492 found a peak in winter over the coastal ECS (Wang et al., 2019). We suggested that the EFs of CDOM

493 and FDOM increased from the coastal regions to the open ocean, and increased from the YS to the

494 ECS were likely due to the enrichment of enough nutrients in the SML in the open ocean promote

495 phytoplankton biomass and DOM production.

496

497

498
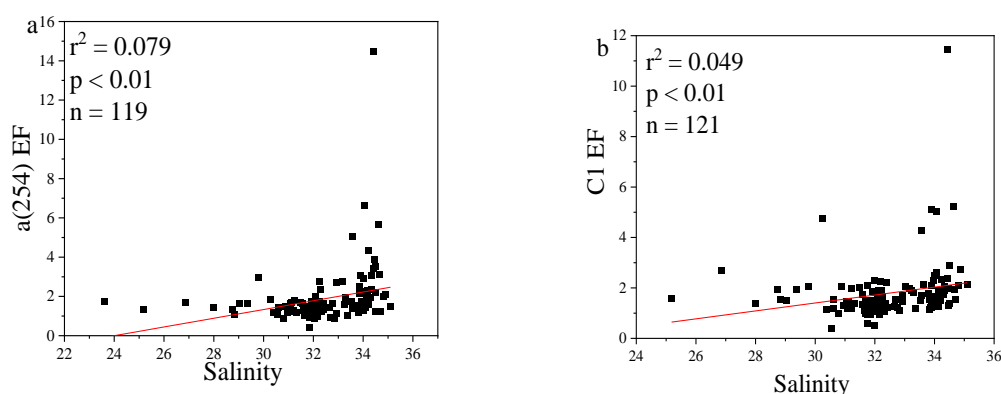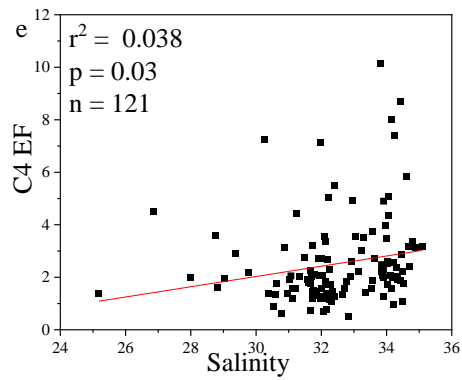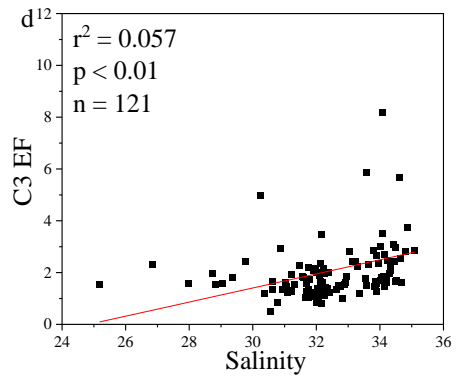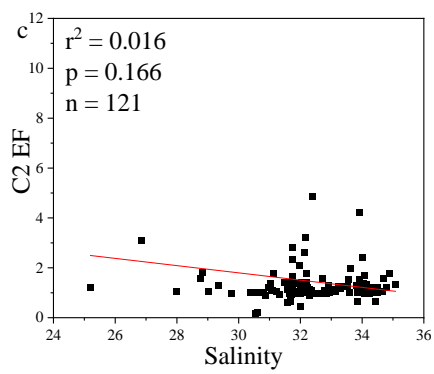
499 Fig. 8. Relationships between salinity and EFs of a(254), Chl-a, DOC, and four fluorescence
500 components.

501   The SML is an aggregate-enriched biofilm environment with distinct microbial communities,

502   where the diversity of microorganisms can differ significantly from those of underlying waters (Liss

503   and Duce, 2005; Cunliffe et al., 2013), the heterotrophic bacterial abundance in the SML was ~ 7.5

504   fold greater than those in the SSW in the ECS during our spring cruise (Sun et al., 2020). Here, EFs

505   showed a greater presence of bacteria and marine protein-like DOM in the SML than that in the SSW,

506   while the protein-like DOM was linked to microbial utilization and degraded faster than the humic-like

507   substances (Yang et al., 2017; Jørgensen et al., 2011). Therefore, compared to coastal waters that have

508   larger terrestrial DOM and nutrients inputs, CDOM shown higher EFs in off-shore regions where

509   DOM in the SSW is mostly of marine autochthonous origin with higher temperatures and stronger

510   biological activity. The significantly higher abundance of cells, phytoplankton, nutrients, and

511   protein-like DOM in the SML supported microbial activities, and further contributing to the local

512   release of marine extracellular DOM directly from microbes in the SML in the off-shore regions.

513   When exposed to higher light intensities (summer), obviously enhance mineralization of DOM in the

514   SML, and relatively less photochemical degradation in SSW could result in lower percentage of

515   aromatic DOM in SML than the SSW. We concluded that SML CDOM dynamics can be expressed as

516   a complex balance among enrichment process, primary production and photochemical destruction.

517   Thus, higher EF of DOM in the SML in off-shore regions are likely supported by a favorable

518   combination of: 1) deposition and accumulation of amphiphilic compounds, 2) importance of bubble

519   for upward transport of DOM and enrichment in SML, and 3) new production of DOM within the

520   SML as a consequence of higher nutrients enrichment and the primary production.

521

522   **4. Conclusions**

523   This study has provided the first data set that considers the distributions of CDOM, FDOM, DOC,

524   Chl-*a*, nutrients, and bacterial abundances in the SML and SSW of the ECS and the YS during spring,

525   summer, and winter. We have observed that the CDOM distribution related variability in primary

526   production in the SML. Furthermore, we have demonstrated that localized and stronger photochemical

527   oxidation may be responsible for the decrease in the aromaticity of the DOM in the SML, due to

528   enhanced transformation or removal of terrestrial DOM, compared with the SSW. We also

529   demonstrated that in off-shore seawaters away from terrigenous influence, the EFs of CDOM, DOC,

530   FDOM and Chl-a in SML tend to be higher in off-shore regions than those in coastal regions, because

531   of the relatively higher enrichment of nutrients which could enhance phytoplankton growth and

532   promoted plant production and DOM production in the SML. Multiple observations of spatial

533   distributions, seasonal variations, chemical compositions, and photochemical reactions of CDOM in

534   the SML have supported the hypothesis that stronger enrichment and photochemical processes occur in

535   the SML in ocean, resulting in relatively accelerated enrichment of more marine local production

536   DOM in the SML than the SSW.

537

538   **Acknowledgements**

539   We thank the captain and crews of the R/V '*Dong Fang Hong 2*', the R/V '*Dong Fang Hong 3*',

540   and the R/V '*Zhe Yu 2*' for their assistance and cooperation during the investigation. We gratefully

541   acknowledge Ya-Hui Gao (Xiamen University), Yu Xin (Ocean University of China), and Xiao-Hua

542   Zhang (Ocean University of China) for providing the Chl-*a*, nutrients, bacterial abundance and

543   picoplankton data, respectively. This work was financially supported by the National Key Research

544   and Development Program (Grant No. 2016YFA0601304), and the National Natural Science

545   Foundation of China (Grant Nos. 41806093 and 491830534).

546

547   **References**

548   Aller, J.Y., Kuznetsova, M., Jahns, C.J., Kemp, P.F., 2005. The sea surface microlayer as a source of

549   viral and bacterial enrichment in marine aerosols. J. Aerosol Sci. 36(5), 801–812.

550   https://doi.org/10.1016/j.jaerosci.2004.10.012

551   Bittar, T.B., Vieira, A.A.H., Stubbins, A., Mopper, K., 2015. Competition between photochemical and

552   biological degradation of dissolved organic matter from the cyanobacteria Microcystis aeruginosa.

553   Limnol. Oceanogr. 2015, 60(4), 1172–1194. https://doi.org/10.1002/lno.10090

554   Breitburg, D., Levin, L.A., Oschlies, A., Grégoire, M., Chavez, F.P., Conley, D.J., Garçon, V., Gilbert,

555   D., Gutiérrez, D., Isensee, K., Jacinto, G.S., Limburg, K.E., Montes, I., Naqvi, S.W.A., Pitcher,

556   G.C., Rabalais, N.N., Roman, M.R., Rose, K.A., Seibel, B.A., Telszewski, M., Yasuhara, M.,

557   Zhang, J., Declining oxygen in the global ocean and coastal waters. Science 2018, 5, 359(6371),

558   eaam7240. https://doi.org/10.1126/science.aam7240

559   Brinkmann, T., Sartorius, D., Frimmel, F.H., 2003. Photobleaching of humic rich dissolved organic

560   matter. Aquat. Sci. 65(4), 415–424. https://doi.org/10.1007/s00027-003-0670-9

561   Brym, A., Paerl, H.W., Montgomery, M.T., Handsel, L.T., Ziervogel, K., Osburn, C.L., 2014. Optical

562   and chemical characterization of base-extracted particulate organic matter in coastal marine

563   environments. Mar. Chem. 162(6), 96–113. https://doi.org/10.1007/s00027-003-0670-9

564   Carlson, C.A., Hansell, D.A., 2003. The contribution of dissolved organic carbon and nitrogen to

565   biogeochemistry of the Ross Sea. In: DiTullio, G., Dunbar, R. (Eds.), Biogeochemical Cycles in

566   the Ross Sea. AGU Press, Washington DC, pp. 123–142.

567   Carpenter, J.H., 1964. The Chesapeake Bay Institute technique for the Winkler dissolved oxygen

568   method. Limnol. Oceanogr. 10(1964), 141–143. https://doi.org/10.4319/lo.1965.10.1.0141

569   Catala, T.S., Reche, I., Fuenteslema, A., Romeracastillo, C., Nietocid, M., Ortegaretuerta, E.,

570   Alvarezsalgado, X.A., 2015. Turnover time of fluorescent dissolved organic matter in the dark

571   global ocean. Nat. Com. 6(1), 5986–5993. https://doi.org/10.1038/ncomms6986

572   Chen, Y., Yang, G., Xia, Q., Wu, G., 2016. Enrichment and characterization of dissolved organic matter

573   in the surface microlayer and subsurface water of the South Yellow Sea. Mar. Chem. 182(Mar.

574   20), 1–13. https://doi.org/10.1016/j.marchem.2016.04.001

575   Chowdhury, S., 2013. Trihalomethanes in drinking water: Effect of natural organic matter distribution.

576   Water SA 39(1), 1–7. https://doi.org/10.4314/wsa.v39i1.1

577   Coble, P.G., 1996. Characterization of marine and terrestrial DOM in seawater using

578   excitation-emission matrix spectroscopy. Mar. Chem. 51(4), 325–346.

579   https://doi.org/10.1016/0304-4203(95)00062-3

580   Coble, P.G., 2007. Marine optical biogeochemistry: the chemistry of ocean color. Chem. Rev. 107(2),

581   402–418. https://doi.org/10.1002/chin.200720265

582   Cunliffe, M., Engel, A., Frka, S., Gasparovic, B., Guitart, C., Murrell, J.C., Wurl, O., 2013. Sea surface

583   microlayers: A unified physicochemical and biological perspective of the air–ocean interface.

584   Prog. Oceanogr. 109(Feb.), 104–116. https://doi.org/10.1016/j.pocean.2012.08.004

585   Danhiez, F.P., Vantrepotte, V., Cauvin, A., Lebourg, E., Loisel, H., 2017. Optical properties of

586   chromophoric dissolved organic matter during a phytoplankton bloom. Implication for DOC

587   estimates from CDOM absorption. Limnol. Oceanogr. 62(4), 1409–1425.

588   https://doi.org/10.1002/lno.10507

589   Dragcevic, D., Pravdic, V., 1981. Properties of the seawater-air interface. 2. Rates of surface film

590   formation under steady state conditions. Limnol. Oceanogr. 26, 492–499.

591   https://doi.org/10.1016/0198-0254(81)91185-7

592   Duce, R.A., Hoffman, G.L., Ray, B.J., Fletcher, I.S., Wallace, G.T., Fasching, J.L., Piotrowicz, S.R.,

593   Walsh, P.R., Hoffman, E.J., Miller, J.M., Heffter, J.L., 1976. Trace metals in the marine

594   atmosphere: Sources and fluxes, in: Marine Pollutant Transfer (H. L. Windom and R. A. Duce,

595   eds.), pp. 77–119, Lexington Books, Lexington.

596   Engel, A., Galgani, L., 2016. The organic sea-surface microlayer in the upwelling region off the coast

597   of Peru and potential implications for air–sea exchange processes. Biogeosciences 13(4),

598   989–1007. https://doi.org/10.5194/bg-13-989-2016

599   Frew, N.M., Bock, E.J., Schimpf, U., Hara, T., Hausecker, H., Edson, J.B., Jahne, B., 2004. Air-sea gas

600   transfer: Its dependence on wind stress, small-scale roughness, and surface films. J. Geophys.

601   Res.-Oceans 109(C8), S17. https://doi.org/10.1029/2003JC002131

602   Galgani, L., Engel, A., 2016. Changes in optical characteristics of surface microlayers hint to

603   photochemically and microbially mediated DOM turnover in the upwelling region off the coast of

604   Peru. Biogeosciences 13(8), 2453–2473. https://doi.org/10.5194/bg-13-2453-2016

605   Garrett, W.D., 1965. Collection of slick-forming materials from the sea surface. Limnol. Oceanogr.

606   10(1965), 602–605. https://doi.org/10.2307/2833459

607   Gonsior, M., Peake, B.M., Cooper, W.T., Podgorski, D., D'Andrilli, J., Cooper, W.J., 2009.

608   Photochemically induced changes in dissolved organic matter identified by ultrahigh resolution

609   fourier transform ion cyclotron resonance mass spectrometry. Environ. Sci. Technol. 43(3),

610   698–703. https://doi.org/10.1021/es8022804

611   Grasshoff, K., Kremling, K., Ehrhardt, M., 2007. Methods of Seawater Analysis, 3rd. Edition. pp.

612   407–420.

613   Guo, W., Yang, L., Zhai, W., Chen, W., Osburn, C.L., Huang, X., Li, Y., 2014. Runoff-mediated

614   seasonal oscillation in the dynamics of dissolved organic matter in different branches of a large

615   bifurcated estuary-The Changjiang Estuary. J. Geophys. Res.-Biogeosciences 119, 776–793.

616   https://doi.org/10.1002/2013JG002540

617 Hansell, D.A., 2013. Dissolved organic carbon reference material program. Eos Transactions

618   American Geophysical Union, 86(35), 308. https://doi.org/10.1029/2005EO350003

619 Hardy, J.T., 1982. The sea surface microlayer: Biology, chemistry and anthropogenic enrichment. Prog.

620   Oceanogr. 11(4), 307–328. https://doi.org/10.1016/0079-6611(82)90001-5

621 Hardy, J.T., Apts, C.W., 1989. Photosynthetic carbon reduction: high rates in the sea-surface

622   microlayer. Mar. Biol. 101(3), 411–417. https://doi.org/10.1007/BF00428138

623 Helms, J.R., Stubbins, A., Ritchie, J.D., Minor, E.C., Kieber, D.J., Mopper, K., 2008. Absorption

624   spectral slopes and slope ratios as indicators of molecular weight, source, and photobleaching of

625   chromophoric   dissolved   organic   matter.   Limnol.   Oceanogr.   53(3),   955–969.

626   https://doi.org/10.4319/lo.2008.53.3.0955

627 Hoge, F.E., Vodacek, A., Blough, N.V., 1993. Inherent optical properties of the ocean: retrieval of the

628   absorption coefficient of chromophoric dissolved organic matter from fluorescence measurements.

629   Limnol. Oceanogr. 38(7), 1394–1402. https://doi.org/10.4319/lo.1993.38.7.1394

630 Jarvis, N.L., 1967. Adsorption of surf ace-active material at the sea-air interface, Limnol. Oceanogr. 12,

631   213–221. https://doi.org/10.4319/lo.1967.12.2.0213

632 Jørgensen, L., Stedmon, C.A., Kragh, T., Markager, S., Middelboe, M., Søndergaard, M., 2011. Global

633   trends in the fluorescence characteristics and distribution of marine dissolved organic matter. Mar.

634   Chem. 126(1–4), 139–148. https://doi.org/10.1016/j.marchem.2011.05.002

635   Kieber, D.J., Mcdaniel, J., Mopper, K., 1989. Photochemical source of biological substrates in sea

636   water: implications for carbon cycling. Nature 341(6243), 637–639.

637   https://doi.org/10.1038/341637a0

638   Kok, M., Schouten, S., Sinninghe Damsté J.S., 2000. Formation of insoluble, nonhydrolyzable,

639   sulfur-rich macromolecules via incorporation of inorganic sulfur species into algal carbohydrates.

640   Geochim. Cosmochim. Acta 64(15), 2689–2699. https://doi.org/10.1016/S0016-7037(00)00382-3

641   Li, Y., He, Z., Yang, G., Wang, H., Zhuang, G., 2019. Volatile halocarbons in the marine atmosphere

642   and surface seawater: Diurnal and spatial variations and influences of environmental factors.

643   Atmos. Environ. 214, 116820. https://doi.org/10.1016/j.atmosenv.2019.116820

644   Liss, P.S., Duce, R.A., 1997. The Sea Surface and Global Change, Cambridge University Press, 519.

645   Liss, P.S., Duce, R.A., 2005. The Sea Surface and Global Change. Cambridge University Press: UK.

646   Liu, S.M., Qi, X.H., Li, X.N., Ye, H.R., Wu, Y., Ren, J.L., Zhang, J., Xu, W.Y., 2016. Nutrient

647   dynamics from the Changjiang (Yangtze River) estuary to the East China Sea. J. Mar. Syst.

648   154(Feb.), 15–27. https://doi.org/10.1016/j.jmarsys.2015.05.010

649   Liu, X., Beusen, A.H.W., Van Beek, L.P.H., Mogollón, J.M., Ran, X., Bouwman, A.F., 2018. Exploring

650   spatiotemporal changes of the Yangtze River (Changjiang) nitrogen and phosphorus sources,

651   retention and export to the East China Sea and Yellow Sea. Water Res. 142(Oct. 1), 246–255.

652   https://doi.org/10.1016/j.watres.2018.06.006

653   Margolin, A.R., Gonnelli, M., Hansell, D.A., Santinelli, C., 2018. Black sea dissolved organic matter

654   dynamics: insights from optical analyses. Limnol. Oceanogr. 63(3), 1425–1443.

655   https://doi.org/10.1002/lno.10791

656   Marie, D., Partensky, F., Jacquet, S., Vaulot, D., 1997. Enumeration and cell cycle analysis of natural

657   populations of marine picoplankton by flow cytometry using the nucleic acid stain SYBR Green I.

658   Appl. Environ. Microbiol. 63(1), 186–193. https://doi.org/10.1109/50.337494

659   Massicotte, P., Asmala, E., Stedmon, C., Markager, S., 2017. Global distribution of dissolved organic

660   matter along the aquatic continuum: Across rivers, lakes and oceans. Sci. Total Environ. 609(Dec.

661   31), 180–191. https://doi.org/10.1016/j.scitotenv.2017.07.076

662   Mcknight, D.M., Boyer, E.W., Westerhoff, P., Doran, P.T., Kulbe, T., Andersen, D.T., 2001.

663   Spectrofluorometric characterization of dissolved organic matter for indication of precursor

664   organic material and aromaticity. Limnol. Oceanogr. 46(1), 38–48.

665   https://doi.org/10.4319/lo.2001.46.1.0038

666   Medeiros, P.M., Seidel, M., Ward, N.D., Carpenter, E.J., Gomes, H.R., Niggemann, J., Dittmar, T.,

667   2015. Fate of the Amazon River dissolved organic matter in the tropical Atlantic Ocean. Global

668   Biogeochem. Cycl. 29(5), 677–690. https://doi.org/10.1002/2015GB005115

669   Mopper, K., Kieber, D.J., 2002. Photochemistry and the cycling of carbon, sulfur, nitrogen and

670   phosphorus. In: Hansell DA, Carlson CA (eds) Biogeochemistry of dissolved organic matter.

671   Academic Press, San Diego, pp. 455–507.

672   Momzikoff, A., Brinis, A., Dallot, S., Gondry, G., Saliot, A., Lebaron, P., 2004. Field study ofthe

673   chemical characterization of the upper ocean surface using various samplers. Limnol. Oceanogr.

674   Methods 2(11), 374–384. https://doi.org/10.4319/lom.2004.2.374

675   Nichols, C.M., Lardière, S.G., Bowman, J.P., Nichols, P.D., Gibson, J.A.E., Guézennec, J., 2005.

676   Chemical Characterization of Exopolysaccharides from Antarctic Marine Bacteria. Microb. Ecol.

677   49(4), 578–589. https://doi.org/10.1007/s00248-004-0093-8

678   Obernosterer, I., Catala, P., Reinthaler, T., Herndl, G.J., Lebaron, P., 2005. Enhanced heterotrophic

679   activity in the surface microlayer of the Mediterranean Sea. Aquat. Microb. Ecol. 39(3), 293–302.

680   https://doi.org/10.3354/ame039293

681   Ogawa, H., Amagai, Y., Koike, I., Kaiser, K., Benner, R., 2001. Production of refractory dissolved

682   organic   matter   by   bacteria.   Science   292(5518),   917–920.

683   https://doi.org/10.1126/science.1057627

684   Orellana, M.V., Matrai, P.A., Leck, C., Rauschenberg, C.D., Lee, A.M., Coz, E., 2011. Marine

685   microgels as a source of cloud condensation nuclei in the high Arctic. Proc. Natl. Acad. Sci.

686   108(33), 13612–13617. https://doi.org/10.1073/pnas.1102457108

687   Ortega-Retuerta, E., Passow, U., Duarte, C.M., Reche, I., 2009. Effects of ultraviolet B radiation on

688   (not   so)   transparent   exopolymer   particles.   Biogeosciences   6(12),   3071–3080.

689   https://doi.org/10.5194/bg-6-3071-2009

690   Osburn, C.L., Handsel, L.T., Mikan, M.P., Paerl, H.W., Montgomery, M.T., 2012. Fluorescence

691   tracking of dissolved and particulate organic matter quality in a river-dominated estuary. Environ.

692   Sci. Technol. 46(16), 8628–8636. https://doi.org/10.1021/es3007723

693   Parsons, T.R., Matia, Y., Lalli, C.M., 1984. A Manual of Chemical and Biological Methods for

694   Seawater Analysis. Pergamon Press, Oxford.

695   Reinthaler, T., Sintes, E., Herndl., G.J., 2008. Dissolved organic matter and bacterial production and

696   respiration in the sea-surface microlayer of the open Atlantic and the western Mediterranean sea.

697   Limnol. Oceanogr. 53(1), 122–136. https://doi.org/10.4319/lo.2008.53.1.0122

698   Romera-castillo, C., Sarmento, H., Alvarezsalgado, X.A., Gasol, J.M., Marrase, C., 2010. Production

699   of chromophoric dissolved organic matter by marine phytoplankton. Limnol. Oceanogr. 55(1),

700   446–454. https://doi.org/10.4319/lo.2010.55.1.0446

701 Sabbaghzadeh, B., Upstill-Goddard, R.C., Beale, R., Pereira, R., Nightingale, P.D., 2017. The Atlantic

702 Ocean surface microlayer from 50 °N to 50 °S is ubiquitously enriched in surfactants at wind

703 speeds up to 13 m s^{-1}. Geophys. Res. Lett. 44(6), 2852–2858.

704 https://doi.org/10.1002/2017GL072988

705 Siegel, D.A., 2005. Colored dissolved organic matter and its influence on the satellite‐based

706 characterization of the ocean biosphere. Geophys. Res. Lett. 32(20), 469–496.

707 https://doi.org/10.1029/2005GL024310

708 Singh, S., D'Sa, E., Swenson, E., 2010. Seasonal variability in CDOM absorption and fluorescence

709 properties in the Barataria Basin, Louisiana, USA. J. Environ. Sci. 22(10), 1481–1490.

710 https://doi.org/10.1016/S1001-0742(09)60279-5

711 State Bureau of Technical Supervision Bureau, 1992. Specifications for Oceanographic Survey-Survey

712 of Biology in Sea Water. Standard Press of China, Beijing, pp. 17–20.

713 Stedmon, C.A., Bro, R., 2008. Characterizing dissolved organic matter fluorescence with parallel

714 factor analysis: a tutorial. Limnol. Oceanogr.-methods 6(11), 572–579.

715 https://doi.org/10.4319/lom.2008.6.572b

716 Stedmon, C.A., Markager, S., 2005. Resolving the variability in dissolved organic matter fluorescence

717 in a temperate estuary and its catchment using PARAFAC analysis. Limnol. Oceanogr. 50(2),

718 686–697. https://doi.org/10.4319/lo.2005.50.2.0686

719 Stedmon, C.A., Markager, S., Bro, R., 2003. Tracing dissolved organic matter in aquatic environments

720 using a new approach to fluorescence spectroscopy. Mar. Chem. 82(3–4), 239–254.

721 https://doi.org/10.1016/s0304-4203(03)00072-0

722 Stedmon, C.A., Markager, S., Tranvik, L., Kronberg, L., Slätis, T., Martinsen, W., 2007.

723 Photochemical production of ammonium and transformation of dissolved organic matter in the

724   Baltic Sea. Mar. Chem. 104(3–4), 227–240. https://doi.org/10.1016/j.marchem.2006.11.005

725   Su, Y., Hu, E., Feng, M., Zhang, Y., Chen, F., Liu, Z., 2017. Comparison of bacterial growth in

726   response to photodegraded terrestrial chromophoric dissolved organic matter in two lakes. Sci.

727   Total Environ. 579(Feb. 1), 1203–1214. https://doi.org/10.1016/j.scitotenv.2016.11.104

728   Sun, H., Zhang, Y.H., Tan, S., Zheng, Y.F., Zhou, S., Ma, Q.Y., Yang, G.P., Todd, J., Zhang, X.H., 2020.

729   DMSP-Producing Bacteria Are More Abundant in the Surface Microlayer than Subsurface

730   Seawater of the East China Sea. Microb. Ecol. 80(1), 350–365.

731   https://doi.org/10.1007/s00248-020-01507-8

732   Wang, F., Feng, T., Guo, Z., Li, Y., Lin, T., Rose, N.L., 2019. Sources and dry deposition of

733   carbonaceous aerosols over the coastal East China Sea: Implications for anthropogenic pollutant

734   pathways and deposition. Environ. Pollut. 245(Feb.), 771–779.

735   https://doi.org/10.1016/j.envpol.2018.11.059

736   Weishaar, J.L., Aiken, G.R., Bergamaschi, B.A., Fram, M.S., Fujii, R., Mopper, K., 2003. Evaluation

737   of specific ultraviolet absorbance as an indicator of the chemical composition and reactivity of

738   dissolved organic carbon. Environ. Sci. Technol. 37(20), 4702–4708.

739   https://doi.org/10.1021/es030360x

740   Weng, H., Tian, R., Ji, Z., Yu, X., 2011. Potential relationships between atmospheric particulate matter

741   transported by winter monsoons and red tides in the East China Sea. Sci. Bull. 56(3), 297–305.

742   https://doi.org/10.1007/s11434-010-4209-x

743   Woolf, D.K., 2005. Bubbles and their role gas exchange, in The Sea Surface and Global Change,

744   edited by P. S. Liss and R. A. Duce, pp. 173–205, Cambridge Univ. Press, U. K

745   Wotton, R.S., Preston, T.M., 2005. Surface Films: Areas of Water Bodies That Are Often Overlooked.

746   Bioscience 55(2), 137–145. https://doi.org/10.1641/0006-3568(2005)055[0137:SFAOWB]2.0.CO

747 Wurl, O., Wurl, E., Miller, L.A., Johnson, K., Vagle, S., 2011. Formation and global distribution of

748   sea-surface microlayers. Biogeosciences 8(1), 121–135. https://doi.org/10.5194/bg-8-121-2011

749 Wurl, O., Holmes, M., 2008. The gelatinous nature of the sea-surface microlayer. Mar. Chem.

750   110(1–2), 89–97. https://doi.org/10.1016/j.marchem.2008.02.009

751 Yamashita, Y., Hashihama, F., Saito, H., Fukuda, H., Ogawa, H., 2017. Factors controlling the

752   geographical distribution of fluorescent dissolved organic matter in the surface waters of the

753   Pacific Ocean. Limnol. Oceanogr. 62(6), 2360–2374. https://doi.org/10.1002/lno.10570

754 Yamashita, Y., 2004. In situ production of chromophoric dissolved organic matter in coastal

755   environments. Geophys. Res. Lett. 31(14), 189–207. https://doi.org/10.1029/2004GL019734

756 Yang, L., Zhang, J., Yang, G.P., 2020. Mixing behavior, biological and photolytic degradation of

757   dissolved organic matter in the East China Sea and the Yellow Sea. Sci. Total Environ. 762(6),

758   143164. https://doi.org/10.1016/j.scitotenv.2020.143164

759 Yang, L., Zhuang, W., Chen, C.A., Wang, B., Kuo, F., 2017. Unveiling the transformation and

760   bioavailability of dissolved organic matter in contrasting hydrothermal vents using fluorescence

761   EEM-PARAFAC. Water Res. 111(Mar. 15), 195–203.

762   https://doi.org/10.1016/j.watres.2017.01.001

763 Zepp, R.G., Sheldon, W.M., Moran, M.A., 2004. Dissolved organic fluorophores in southeastern US

764   coastal waters: correction method for eliminating Rayleigh and Raman scattering peaks in

765   excitation–emission matrices. Mar. Chem. 89(1), 15–36.

766   https://doi.org/10.1016/j.marchem.2004.02.006

767 Zhu, W.Z., Yang, G., Zhang, H., 2017. Photochemical behavior of dissolved and colloidal organic

768   matter in estuarine and oceanic waters. Sci. Total Environ. s607–608(Dec. 31), 214–224.

769   https://doi.org/10.1016/j.scitotenv.2017.06.163

Table 1 Spectral characteristics of the four fluorescent components identified by the PARAFAC

modal in this study, compared with those preciously identified.

Component	Ex_{max} (nm)	Em_{max} (nm)	Coble (1996)	Comparison with other studies using PARAFAC	Description and probable source
C1	345	455	peak C 320-360/420-480	Osburn et al. (2012)	Terrestrial-like humic substances
C2	255	310 (375)	peak A 230-260/380-460	Stedmon et al. (2003)	Tyrosine-like or marine humic-like substances
C3	315	385	peak M 290-310/370-420	Stedmon and Markager (2005)	Marine humic-like substances (biological degradation)
C4	280	335	peak T 270-280/340-350	Coble (1996)	Tryptophan-like; Non-Humic-like; Biological production in the water column

Table 2 Average temperature, salinity, wind speed, CDOM a(254), DOC, Chlorophyll-*a* (Chl-*a)*, dissolved oxygen (DO), $S_{275-295}$, S_R, and SUVA$_{254}$ of the SSW and SML in the YS and ECS during spring, summer, and winter.

	Water layer	Spring mean	Spring SD	Summer mean	Summer SD	Winter mean	Winter SD
Temperature (℃)	SSW	14.0	4.91	24.0	3.66	14.0	5.23
Salinity	SSW	32.5	1.92	31.7	2.17	32.7	1.41
Wind Speed (m s^{-1})	SSW	5.98	2.86	5.47	2.51	6.09	2.52
DO (mg L^{-1})	SSW	6.44	0.85	7.57	1.07	8.32	0.99
Chl-*a* (μg L^{-1})	SSW	1.26	2.38	1.13	1.48	0.42	0.25
	SML	1.63	3.66	1.28	1.13	no data	
DOC (μmol L^{-1})	SSW	91.3	25.7	109.4	33.55	88.4	22.51
	SML	132.9	77.4	145.7	49.8	131.3	91.1
a(254) (m^{-1})	SSW	3.20	2.49	3.10	1.34	2.52	1.26
	SML	3.70	1.98	4.05	1.66	4.74	2.50
$S_{275-295}$ (nm^{-1})	SSW	0.0201	0.0049	0.0188	0.0035	0.0207	0.0068
	SML	0.0222	0.0073	0.0178	0.0021	0.021	0.0055
S_R	SSW	1.723	1.026	1.731	1.557	1.521	0.52
	SML	1.095	0.218	1.361	0.296	1.416	0.214
SUVA$_{254}$ (L mg-C^{-1} m^{-1})	SSW	2.067	0.664	2.244	0.671	3.008	0.949
	SML	1.911	0.768	1.951	0.359	2.992	1.034

Table 3 Correlation coefficients between EF of DOM optical properties, Chl-a, DOC, PO_4^{3-}, NO_3^-,

NO_2^-, SiO_3^{2-}, Cyanobacteria, Picophytoplankton, Bacterial abundance.

	EF of a(254)	EF of DOC	EF of Chl-a	Ef of C1	EF of C2	EF of C3	EF of C4	EF of PO_4^{3-}	EF of NO_3^-	EF of NO_2^-	EF of SiO_3^{2-}	EF of Cyanobacteria	EF of picophytoplankton
EF of DOC	0.185												
EF of Chl-a	0.092	0.021											
Ef of C1	**.336****	0.047	-0.119										
EF of C2	0.163	0.073	-0.017	**.635****									
EF of C3	**.413****	0.179	-0.096	**.907****	**.557****								
EF of C4	**.319****	0.021	0.011	**.574****	**.368****	**.628****							
EF of PO_4^{3-}	0.129	0.267	**.319***	0.131	-0.037	0.139	0.087						
EF of NO_3^-	-0.065	-0.054	0.235	-0.037	-0.044	-0.027	-0.053	0.26					
EF of NO_2^-	0.15	0.208	**.307***	0.142	-0.017	0.192	0.035	**.571****	0.271				
EF of SiO_3^{2-}	**.634***	0.004	0.074	0.122	-0.101	0.305	0.151	0.205	-0.118	-0.141			
EF of Cyanobacteria	0.091	-0.017	0.028	-0.027	-0.105	-0.047	-0.052	0.218	0.027	**.755****	-0.286		
EF of Picophytoplankton	**.347****	0.0281	0.252	-0.067	-0.082	-0.077	0.025	0.218	-0.08	0.113	-0.327	0.081	
EF of Bacterial abundance	-0.036	-0.069	-0.063	-0.061	0.004	0.014	-0.093	-0.12	-0.026	-0.073	-0.099	**.730****	-0.064

** Correlation is significant at the 0.01 level (two-tailed)

* Correlation is significant at the 0.05 level (two-tailed)